SCANNING TRANSMISSION X-RAY AND FLUORESCENCE MICROSCOPY OF LIPID BILAYERS

SCANNING TRANSMISSION X-RAY AND FLUORESCENCE MICROSCOPY OF LIPID BILAYERS

By: Jonathan Daniel West, B. S.

A Thesis
Submitted to the School of Graduate Studies in Partial Fulfillment of the Requirements for the Degree Master of Science

McMaster University

MASTER OF SCIENCE (2016)   McMaster University
Chemistry & Chemical Biology, Hamilton, Ontario

TITLE: Scanning Transmission X-Ray and Fluorescence Microscopy of Lipid Bilayers

AUTHOR: Jonathan D. West, B.S. (Wake Forest University)

SUPERVISORS: Professors Adam P. Hitchcock and José M. Moran-Mirabal

NUMBER OF PAGES: 98

Abstract

Cationic antimicrobial peptides (cAMPs) are of interest as a possible solution to the problem of bacterial resistance to antibiotics. In order to facilitate identification of useful cAMPs, the mechanism of action in killing prokaryotic cells is of interest. Robert Hancock (UBC) has proposed that charge interaction between cAMPs and the negatively-charged bacterial membrane is a major factor that contributes to the disruption of the bacterial membrane. The goal of this thesis is to contribute to the development of a method based on scanning transmission X-ray microscopy (STXM) to investigate the electrostatic interaction hypothesis as the method by which cAMPS interact with negatively charged bacterial membranes, using fluorescence microscopy (FM) as a guide. Methods were developed to generate phase-segregated lipid bilayers as model membranes on the silicon nitride membranes. C 1s, N 1s and O 1s X-ray absorption spectra of 3 lipid species - 1,2-di-(9Z-octadecenoyl)-*sn*-glycero-3-phosphocholine (DOPC), 1,2-dioctadecanoyl-*sn*-glycero-3-phosphocholine (DSPC), and 1,2-di-(9Z-octadecenoyl)-3-trimethylammonium-propane (chloride salt) (DOTAP) were obtained to be used as reference standards in future studies. FM and STXM were used to map the saturated and unsaturated domains in dried lipid bilayers exhibiting phase segregation. Attempts were also made to image the lipid bilayers under hydrated conditions using both static and flow cells. Efforts to develop a flow cell for STXM using 3D printing are outlined. The potential to evolve this line of research to enable systematic studies of protein and peptide interactions with lipid bilayers under static and dynamic conditions is discussed.

Acknowledgements

I would first like to thank my supervisors, Drs. José Moran-Mirabal and Adam Hitchcock for their guidance and expertise during my graduate studies. I sincerely appreciate the help and guidance during my master's. I would like to thank you both for making both laboratories a warm and collaborative environment in which I was able to both study and conduct research among a great group of lab mates. Thank you to Yujie Zhu, who did the pioneering work on this project and for all her help throughout the course of my master's. I would like to thank the beamline staff at the Advanced Light Source and the Canadian Light Source for being so helpful during my experiments there. Specifically, I would like to thank Drs. Jian Wang, David Kilcoyne and Young-Sang Yu. Thank you to Hooman Hosseinkhannazer from Norcada (Edmonton, Alberta) who provided the hydrophilic coated silicon nitride windows that helped the lipid bilayer preparation. I would also like to thank my group members for their support and encouragement. Thank you Dr. Glyn Cooper, Dr. Narayana Appathurai, Xiaohui Zhu, Juan Wu, Lis Melo, Vinod Prabu, Justin Boyle, Travis Sutherland, Sanjay Sonney, Ayodele Fatona, Kevin Saem, and Urooj Gil.

Software used in this Thesis

- aXis 2000 (Analysis of X-ray Images and Spectra)
  - Developed by Chris Jacobsen, Carl Zimba, Peter Hitchcock and Adam Hitchcock et al. It is maintained by Adam Hitchcock and is available for free download (for non-commercial use) at http://unicorn.mcmaster.ca/aXis2000.html
- SigmaPlot 2000 for Windows Version 6.10 Copyright© 1986-2000 SPSS Inc.
- Image J 1.49v
  - Wayne Rasband
  - National Institute of Health, USA
  - http://imagej.nih.gov/ij
  - Java 1.6.0_24 (64-bit)
  - Image J is in the public domain
- Autodesk® Inventor Professional 2015

TABLE OF CONTENTS

List of Figures

List of tables

Definitions of Acronyms

ABS- Acrylonitrile Butadiene Styrene
ALS- Advanced Light Source
AMP- Antimicrobial Peptide
CAD- Computer Aided Design
CAMP- Cationic Antimicrobial Peptide
CCD- Charge Coupled Device
CLS- Canadian Light Source
DHPE-LR- Lissamine Rhodamine B 1,2-dihexadecanoyl-sn-glycero-3-phosphoethanolamine, triethylammonium Salt
DI- Deionized Water
DiI- (1,1'-Dioctadecyl-3,3,3',3'-Tetramethylindocarbocyanine Perchlorate ('DiI'; $DiIC_{18}(3)$))
DOPC- 1,2-di-(9Z-octadecenoyl)-*sn*-glycero-3-phosphocholine
DSPC- 1,2-dioctadecanoyl-*sn*-glycero-3-phosphocholine
DOPS- 1,2-dioleoyl-*sn*-glycero-3-phospho-L-serine (sodium salt)
DOTAP- 1,2-di-(9Z-octadecenoyl)-3-trimethylammonium-propane (chloride salt)
EELS- Electron Energy Loss Spectroscopy
FM- Fluorescence Microscopy
FRAP- Fluorescence Recovery after Photobleaching
HIPS- High-Impact Polystyrene
HPLC- High Performance Liquid Chromatography
LMV- Large Multilamellar Vesicles
MSDS- Material Safety Data Sheets
NEXAFS- Near-Edge X-ray Absorption and Fine Structure
NMR- Nuclear Magnetic Resonance
OD- Optical Density
OD1- Optical Density per Nanometer
OSA- Order Sorting Aperture
PBS- Phosphate-buffered Saline
PEEK- Polyetheretherketone
PGM- Plane Grating Monochromator
PLA- Polylactic Acid
SCCM- Standard Cubic Centimeters Per Minute
SiN$_x$- Silicon Nitride
SLB- Supported Lipid Bilayer
SM- Spectromicroscopy
STXM- Scanning Transmission X-ray Microscopy
SUV- Small Unilamellar Vesicle
TEM- Transmission Electron Microscopy
XAS- X-ray Absorption Spectroscopy
XPS- X-ray Photoelectron Spectroscopy
ZP- Zone Plate

1. Introduction

Although antibiotics have been used as effective first line treatments against bacterial infections since their widespread adoption in the 1930s, the ability of target bacteria to develop resistance to them has limited their utility [WHO, 2015]. A notable example of the phenomenon of bacterial resistance is penicillin, which was famously discovered serendipitously by Alexander Fleming in 1928 [ACS, 2015]. Penicillin was used for decades with great efficacy against many different bacterial species, but has recently become less effective against thwarting bacterial species [Alekshun 2007]. This is thought to have been caused by the increased bacterial resistance to penicillin [Alekshun, 2007, Larson, 2007].

1.a Antimicrobial Peptides

Antimicrobial peptides (AMPs) have been investigated as potential alternatives to classic antibiotic therapies to alleviate the problem of antibiotic resistance. AMPs are present in the innate immune system of all phyla of life [Reddy, 2004]. AMPs have demonstrated their efficacy against many species that have the potential to cause human illness, including: viruses, fungi, Gram positive and negative bacteria, and cancerous cells [Reddy, 2004].

1.a.1 Structure

AMPs range in length from about 12 to 50 amino acid residues and can differ at all four hierarchies of protein structure [Yeaman, 2003]. AMPs are typically classified by their secondary structure which can take four forms: α-helical, β-hairpin (when there is only one disulfide bond present), β-stranded (when there are at least 2 disulfide bonds present), or extended structure [Dhople, 2006]. AMPs remain unfolded in solution but once they interact with biological membranes they fold into their final configuration [Dhople, 2006].

1.a.2 Mechanisms

AMPs are believed to interact with invading agents by several mechanisms [Nguyen, 2011] –

Figure 1.1. The specific mechanism depends on the amino acid composition, amphipathicity,

size, and charge of the AMP [Brogden, 2005]. Proposed mechanisms include the barrel-stave,

toroidal-pore, and carpet mechanism [Brogden, 2005]. In the barrel-stave mechanism, many

channel-forming peptides position themselves like a round barrel around an aqueous pore,

where lone peptides or peptide complexes have inserted into the bilayer [Brogden, 2005]. The

toroidal-pore mechanism differs from the barrel-stave in that peptides with an α-helical structure

interact with the hydrophobic and charged bilayer. Hydrophobic residues of the peptides replace

the polar head groups, which creates a hole in the hydrophobic region and causes a strain in the

membrane. It is this strain which modifies the membrane surface, allowing for further peptide

interactions with the membrane [Brogden, 2005]. In the carpet mechanism, AMPs diffuse across

the membrane in a similar way to a detergent molecule. Peptides are accumulated on the surface

of the bilayer through electrostatic interactions and compromise the integrity of the membrane

by changing the fluidity of the membrane [Brogden, 2005].
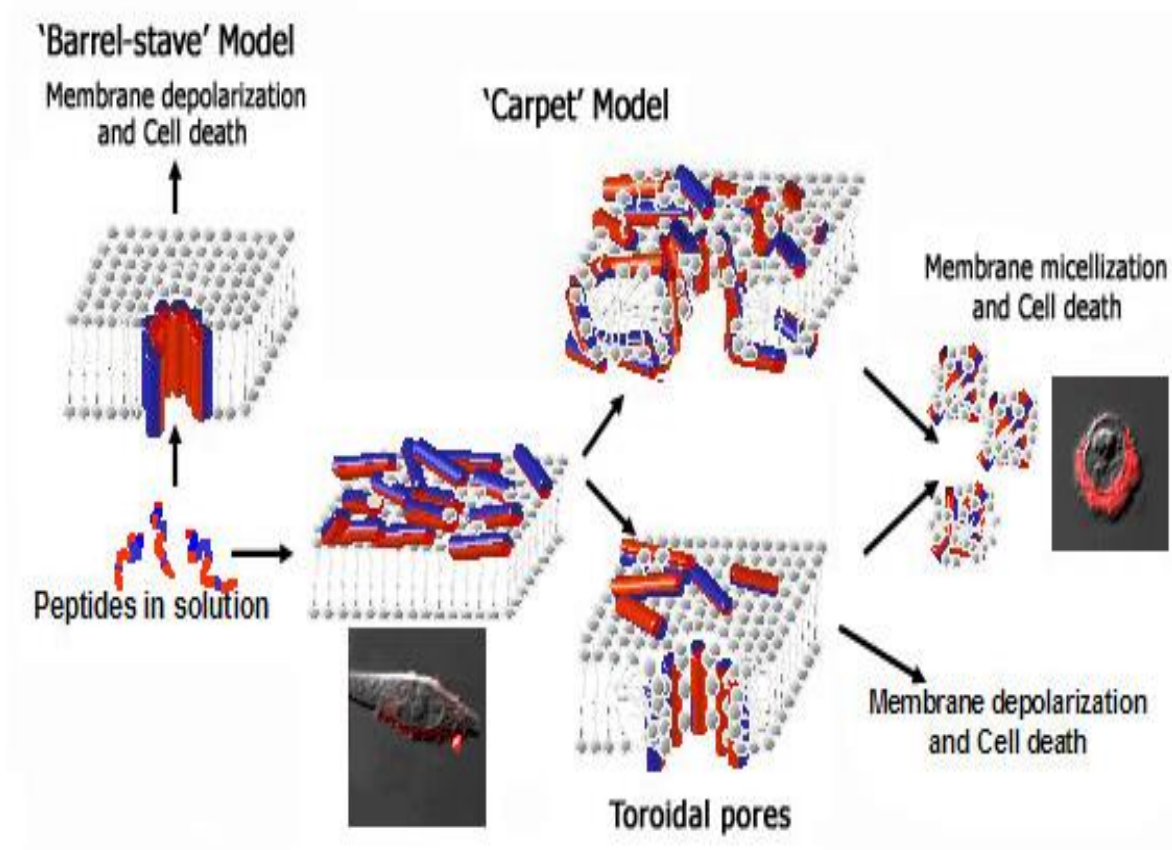
Figure 1.1. *Barrel-stave, toroidal pore, and carpets models of peptide/membrane interactions. Adapted from Papo, N., and Y. Shai (2005).*

1.a.3 Selectivity and Resistance

The selectivity of AMPs is dictated by their cationic properties [Matsuzaki, 2009]. The surfaces of bacterial membranes tend to be more negatively charged than those of mammalian cells [Hancock, 2006]. This difference in charge is believe to account for the fact that AMPs have different binding affinities for prokaryotic and eukaryotic membranes. Electrostatic attraction between positively charged cationic antimicrobial peptides (cAMPs) and negatively charged prokaryotic membranes is postulated to be critical to the mechanism of action of CAMPs [Hancock, 2006] – Figure 1.2. The difference in charge between the outside and inside of the membrane, the membrane potential, affects peptide-lipid interactions [Matsuzaki, 1995]. The greater negative membrane potential of bacteria makes them vulnerable to attack from cationic antimicrobial peptides (cAMPs) because cAMPs can diffuse into the membrane more readily [Matsuzaki, 1995]. Cholesterol, which is present in eukaryotic membranes but not in prokaryotic membranes, also influences the binding of cAMPs [Zasloff, 2002]. This arises either because of the stabilizing interaction of the cholesterol with the lipid bilayer, or the interaction between the cholesterol and the peptide [Zasloff, 2002].
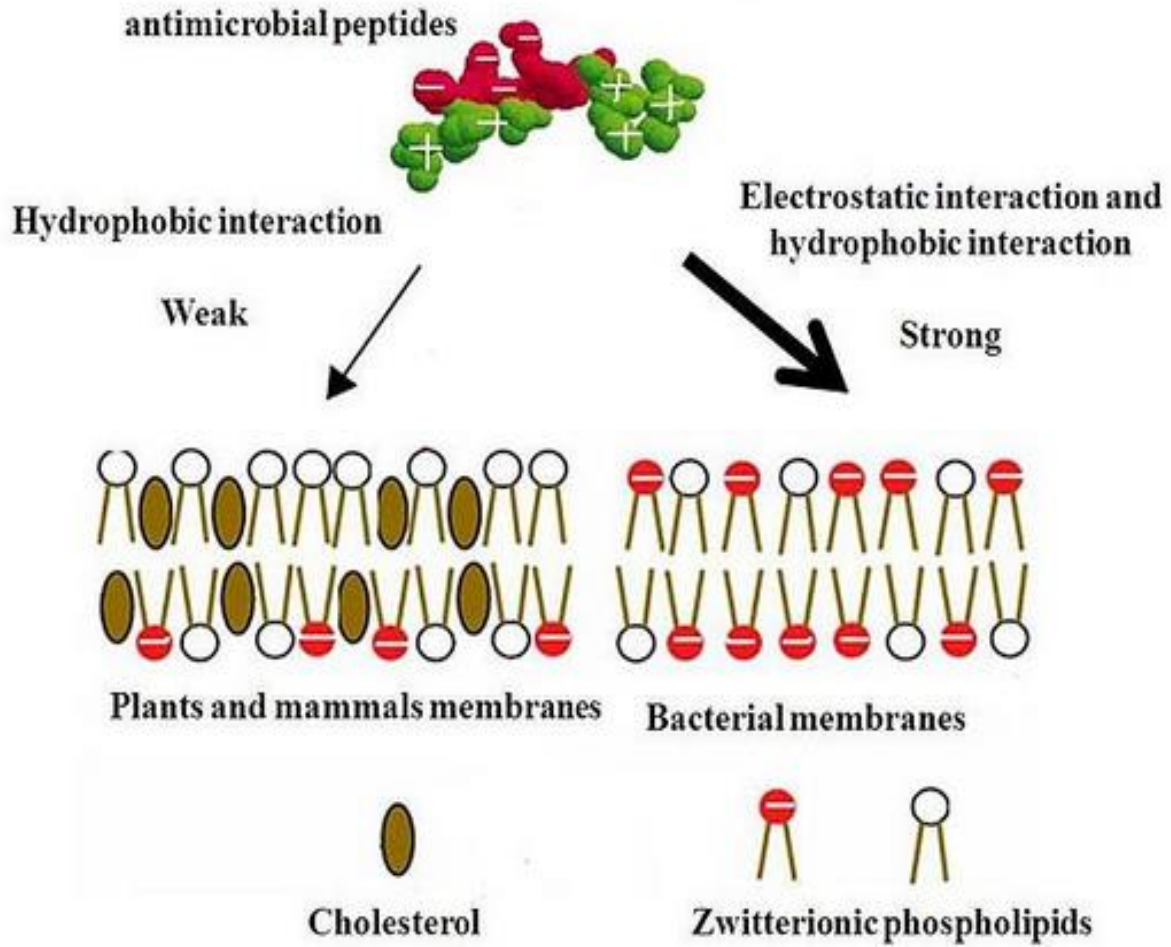
Figure 1.2. *Illustration of charge/membrane potential of lipids and its effects on peptide/lipid interactions. Adapted from Zasloff, M. (2002)*

The discussion of peptide selectivity is directly related to bacterial resistance to cAMPs. If peptides attack healthy host cells, then their purpose is defeated. This is perhaps the greatest drawback to their widespread use. If bacteria become resistant to peptides and, specifically, if that resistance causes the body's immune system to become vulnerable to attack from the AMPs, clearly, this would be a major problem. If large amounts of cAMPs are given as treatment, this facilitates the selective survival of bacteria resistant to cAMPs which, in turn, would permit the bacteria to become more resistant to the body's immune system [Habets, 2012]. Studies have shown that bacteria are capable of developing strategies to resist cAMPs [Brogden, 2005]. The exact mechanisms by which antibiotic resistance occurs depend on the specific bacterial species, but one mechanism that may increase bacterial resistance is a change of the surface charges on the bacterial cell membrane [Habets, 2012]. For example, *Staphylococcus aureus* has been shown to increase the overall positive charge of its membrane by adding L-lysine residues [Peschel, 1999].

Although there are concerns with employing AMPs as therapeutic agents, there are many benefits as well. AMPs are not bacteriostatic (an agent which merely stops bacteria from growing), they are bactericidal and can quickly induce cell apoptosis [Reddy, 2004]. Studies have shown the potential effectiveness of AMPs for conditions ranging from lung infections secondary to cystic fibrosis, to skin infections, and even to certain types of cancer [O'Driscoll, 2012, Hoskin, 2008]. Research is underway to control the selectivity of AMPs so they do not harm healthy cells or result in antibiotic resistance, a growing concern [Matsuzaki, 1995, Peters, 2010].

1.b Lipid Bilayers

This project seeks to outline the interactions between AMPs and lipid bilayers. Therefore, the construction of a model lipid bilayer system that resembles a prokaryotic bilayer membrane is necessary for this experiment. The detailed procedure for the formation of a lipid bilayer is discussed in Chapter 2. Figure 1.3 describes the nomenclature of the vesicles and the types of bilayers that can be constructed. The lipid vesicles are reduced in size throughout the procedure, from giant unilamellar vesicles (GUVs) to large unilamellar vesicles (LUVs) then to small unilamellar vesicles (SUVs). The SUVs were used to form solid supported lipid bilayers (SLBs) on various substrates (SiO_2, SiN_x and mica) and can also be used to form tethered supported lipid bilayers (tSLBs).

SUV
<100 nm

LUV
100-1000 nm

GUV
>1 µm

Multilamellar

a

b

c

Phospholipid
Head Groups

Hydrophobic
Membrane
Interior

Phospholipid
Head Groups

Solid Supported Lipid Bilayer

Phospholipid
Head Groups

Hydrophobic
Membrane
Interior

Aqueous Sub-
membrane
Space

Tethered Lipid Bilayer
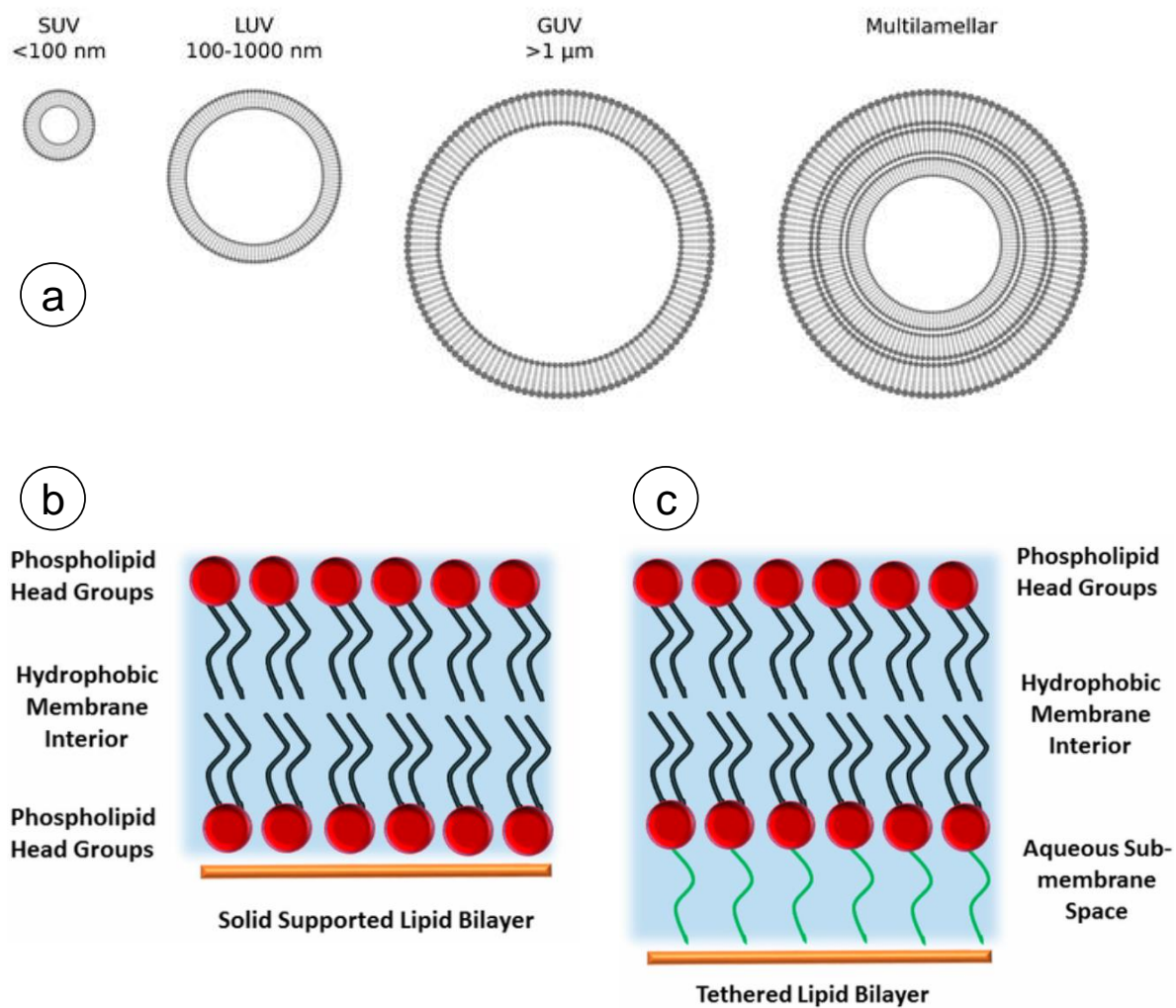
Figure 1.3. *Illustration of lipid vesicles sizes and an SLB formed on the surface of a support. Adapted from Andersson, J (2016) and van Swaay, D (2013).*

1.c Techniques

Many techniques have been used to investigate AMP and their interactions with membranes, including: fluorescence microscopy, atomic emission spectroscopy, neutron and X-ray diffraction, solid-state NMR spectroscopy, dual polarization interferometry, solid-state NMR, and visible light microscopy [Brogden, 2005, Korlach et al 1999]. Studies employing solid-state NMR have determined how AMPs disrupt membranes at the atomic level [Henzler, 2003]. Dual polarization interferometry, which makes use of an evanescent wave from a laser, has been used to analyze the conformational changes AMPs undergo when binding to the surface of lipid bilayers [20]. Core level X-ray absorption spectroscopy and its associated implementation as spectromicroscopy in various types of soft X-ray microscopes [Hitchcock, 2012] has been previously used to study biological samples containing lipid and other biological materials. Lawrence et al (2003) used scanning transmission X-ray microscopy (STXM) in comparison to confocal fluorescence microscopy to measure lipid distributions in natural environmental biofilms. Won et al (2011) and Leung et al (2010, 2011) used X-ray photoemission electron microscopy (X-PEEM) and STXM to characterize AMP /lipid bilayer interactions. The current project made use of scanning transmission X-ray microscopy and fluorescence microscopy as the main analytical methods.

2. Experimental

2.a Scanning Transmission X-Ray Microscopy

Scanning Transmission X-ray Microscopy (STXM) is a synchrotron-based technique which measures near-edge X-ray absorption fine structure (NEXAFS) with high spatial resolution [Howells, 2007]. The best spatial resolution that STXM is has achieved is 10 nm, which allows STXM to achieve molecule-specific spectroscopy [Chao, 2012]. STXM is advantageous compared to other analytical techniques because the amount of radiation damage per analytical information obtained is approximately two orders of magnitude lower than core level electron loss spectroscopy (EELS) performed in a transmission electron microscope [Rightor, 1997, Wang, 2009].

All STXM data presented in this report were measured at either undulator beamline 10.ID.1 at the Canadian Light Source (CLS) in Saskatoon, Saskatchewan, or bend magnet beamline 5.3.2.2 at the Advanced Light Source (ALS) in Berkeley, California.

At the ALS polymer microscopy beamline, X-rays are taken from ~ 15% of the output of bend magnet 5.3, the 3rd bend magnet of 1 sector triple bend achromat that guides the electrons around the 1.9 GeV storage ring. These X-rays are focused in the horizontal direction at the entrance slit and in the vertical direction on the exit slit of a spherical grating monochromator (**Figure 2.1.a**.) The simple 2-optic design provides high efficiency and stability, in part due to a piezo feedback system on the toroidal focusing mirror, which keeps the illumination of the zone plate very stable. The 5.3.2.2 beamline also has a N_2 gas filter which improves C 1s spectroscopy by eliminating 2nd order light [Warwick, 2002].
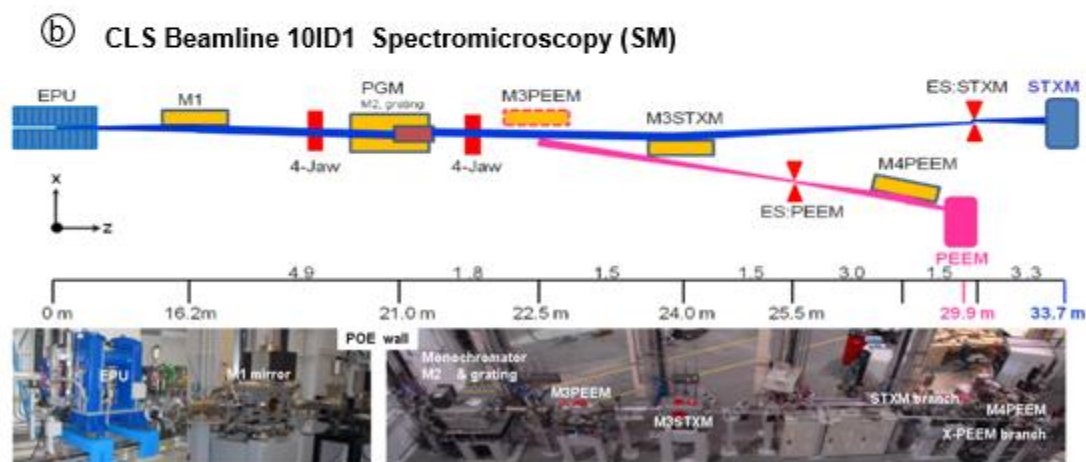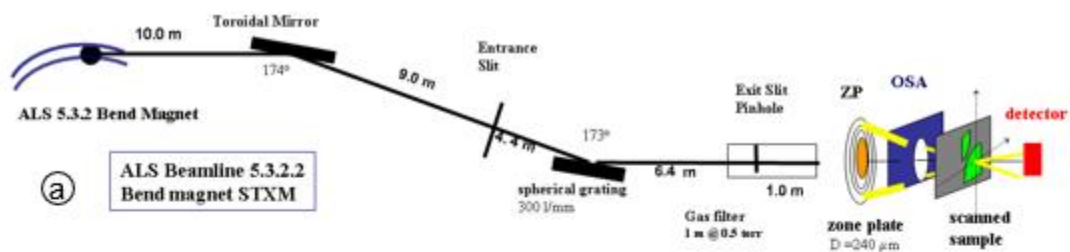
Figure 2.1a *Schematic of the ALS beamline 5.3.2.2 Bend Magnet STXM*

Figure 2.1b *Schematic and images of the undulator beamline 10.ID.1 at the CLS*

At the CLS spectromicroscopy (SM) beamline X-rays are generated by an elliptically polarizing undulator (EPU) in straight section 10 of the 2.9 GeV storage ring. The EPU is comprised of four quadrant arrays of permanent magnets that can change the polarization of radiation by changing the positions of the girders. The electromagnetic radiation produced by the EPU is conditioned by focusing, collimating and dispersing optics, before arriving at the STXM end station (**Fig. 2.1.b**). CLS-SM has a Ti filter in the beamline to reduce 2nd order light to improve C 1s spectroscopy [Kaznatcheyev, 2009]. In both the ALS and CLS systems the exit slit acts both as an energy band-pass selector and to define the coherence of the light, which directly impacts the spatial resolution.

Figure 2.2 outlines the features of the interferometer-based STXM used at both ALS 5.3.2.2 and CLS-SM [Kilcoyne, 2003]. The monochromatic and partially coherent X-rays that reach the STXM are focused by a Fresnel zone plate, which is a circular diffraction grating [Attwood, 2000]. The zone plate focuses the X-ray beam to a highly collimated spot at which the sample is positioned. In order to prevent zero-order (un-diffracted light) from hitting the sample, a combination of an X-ray opaque central stop (CS) and an order-sorting aperture (OSA) centered on the CS are used. STXM images are generated by raster-scanning the sample in the x-y plane, while detecting the X-rays transmitted through the sample in single photon counting mode using a custom phosphor plate and a high performance photomultiplier detector (Hamamatsu R647P).
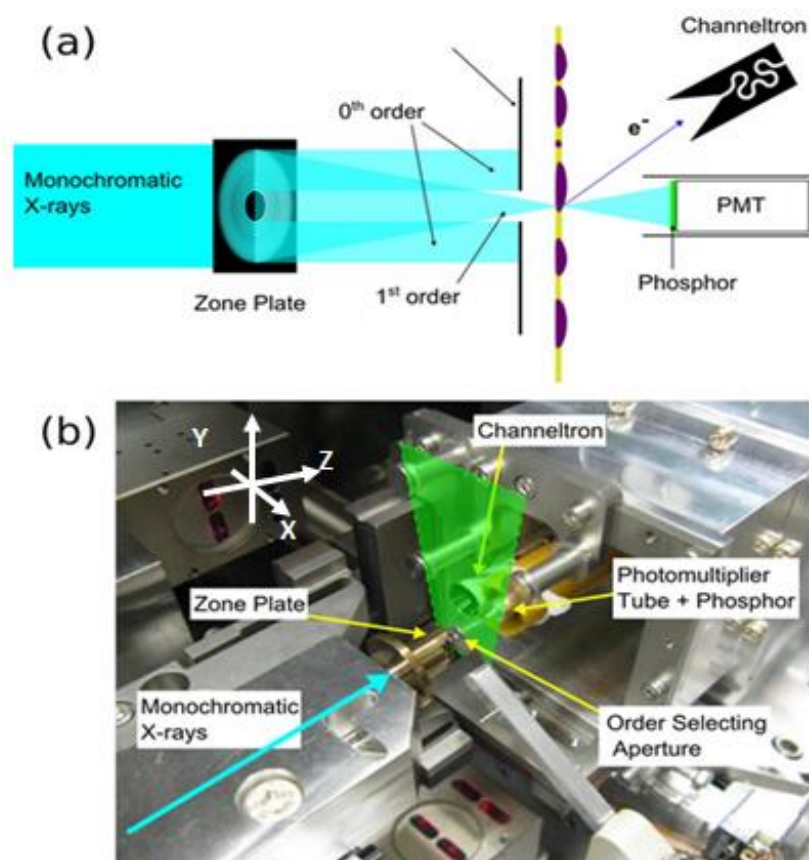
Figure 2.2. STXM Layout and sample positioning. (a) Schematic diagram of STXM. (b) Photograph of the major components of STXM. The area in green shows where the sample plate attaches to the three-pin holder. Adapted from Xiaohui Zhu (2014).

2.b Lipid Reference Spectroscopy Sample Preparation

All lipids were purchased from Avanti Polar Lipids (Alabaster, Alabama) in powder form, dissolved

in HPLC-grade chloroform to a stock concentration of 25 mg/mL and stored in glass vials sealed

with Teflon coated caps. The vials were then sealed using Parafilm™ from Bemis Company, Inc.

(Neenah, Wisconsin) and stored at −10°C until needed. To remove organic contaminants, all

glassware and substrates used for lipid sample preparation were cleaned using Piranha solution

(5:1 v/v H_2SO_4(concentrated):H_2O_2(30%)) at 100-110°C for 10 minutes and rinsed copiously with

18.2MΩ water (A10-Merck-Millipore system, Darmstadt, Germany).[1] Lipid samples for

spectroscopy were prepared in clean 2 mL glass vials using the stock lipid solutions. The amount

of each lipid placed into the vial was calculated based on the desired molar fractions of the lipid

components to obtain a total lipid content of 1 µmol. The lipid mixtures were then dried under

an Argon stream to form lipid cakes at the bottom of the vials, which were then placed uncapped

in a vacuum oven at 40°C (Thermo Scientific 3625A-1 Hi- Temp Vacuum, Waltham,

Massachusetts) and left overnight to ensure the chloroform was completely removed. 1 mL of

18.2MΩ water (TOC ≥ 3 ppb) was added to each vial to yield lipid solutions at 1mM concentration.

The lipid cakes were hydrated through vigorous mixing using a vortex stirrer (Fisher Scientific,

Analog Vortex Mixer, Waltham, Massachusetts) to generate large multilamellar vesicles (LMVs).

Small unilamellar vesicles (SUVs) were subsequently produced by reducing the size of the LMVs

through 5 minute point-probe sonication using a Branson Cell Dismembrator (Model 705 with

sound enclosure, Branson Ultrasonics Corporation, Danbury, Connecticut) operated at 60%

---

[1] **Safety note:** the mixture of H_2SO_4 and H_2O_2 reacts exothermically, so care must be exercised when preparing the solution and heating it up to the cleaning temperature.

maximum amplitude using a 2 inch cup horn. The SUV solutions were diluted to 5 µM concentration with 18.2MΩ water and then drop-cast onto SiN_x windows (Norcada) that had been cleaned using piranha solution [Zhu, 2014] followed by 30 s plasma oxidation (30 sccm air inlet flow, 600 mTorr) at high power setting (30 W) in a PDC expanded plasma cleaner (Harrick, Ithaca, NY). SiN_x refers to a silicon nitride window with an unknown empirical formula. Silicon nitride is known to have an empirical formula of Si_3N_4, but studies have shown that heating and storage of silicon nitride windows oxidizes the surface and changes the empirical formula, so SiN_x is used as a general formula (Oh, 2016). The low lipid solution concentration was chosen to produce single lipid layers on the SiN_x windows. The piranha cleaning followed by plasma oxidation made the SiN_x window surface hydrophilic, which facilitated spreading of the lipid solution over the full window area. SiN_x windows were secured to STXM sample plates using 3M doubled-sided tape (Two Harbors, Minnesota). The SiN_x windows were handled only at the corners of the frame with clean tweezers and leveled on the double-sided tape by lightly pressing down on the corners of the window frame. Lipid solutions were added to the SiN_x windows using appropriately sized plastic pipette tips for aqueous solutions, or glass syringes (Hamilton Company Reno, Nevada) for chloroform solutions, to ensure chloroform would not dissolve the plastic and contaminate the sample. The samples were imaged in a fluorescence optical microscope (Nikon Eclipse E600 equipped with a RETIGA 2000R CCD Camera Tokyo, Japan), to aid with identification of suitable areas for STXM.

2.c Characterization of Supported Lipid Bilayers using Fluorescence Microscopy

Supported lipid bilayer (SLB) samples were imaged in 1X (1mM) phosphate-buffered saline (PBS) using a Nikon Eclipse LV100N POL epifluorescence microscope (Nikon Instruments,

Mississauga, ON, USA) equipped with excitation and emission filters for Rhodamine B dye, and a physiological CFI Plan Fluor 60×/0.85NA objective. Images were acquired with a Retiga 2000R cooled CCD camera (QImaging, Surrey, BC, Canada) and recorded with the software NIS-Elements AR (Nikon, Tokyo, Japan). Fluorescence recovery after photobleaching (FRAP) tests were performed to confirm the formation of a bilayer on the substrate and test the mobility of the supported lipid bilayers (SLBs).

2.d Lipid Bilayer Formation Procedure

The lipids used to prepare the DOPC/DSPC bilayer sample were purchased from Avanti Polar Lipids (Alabaster, Alabama). Lissamine Rhodamine B 1,2-dihexadecanoyl-sn-glycero-3-phosphoethanolamine, triethylammonium salt (DHPE-LR) was purchased from Life Technologies (Carlsbad, California) for use as a fluorescent probe to allow for fluorescence imaging of the DOPC in the bilayer. The three components, DOPC, DSPC and DHPE-LR were mixed in chloroform in 10:90:0.1, 25:75:0.1, 50:50:0.1, 75:25:0.1, and 90:10:0.1 molar ratios respectively in a piranha cleaned glass vial. The ratio of the two main lipid components was varied to control the amount of lipid within each phase and the size of the discrete DSPC domains, as discussed below. Chloroform was removed using an argon stream and the lipid cake was left to dry overnight in a vacuum oven. The lipid cake was hydrated with the necessary volume of 1X PBS to generate a 1mM concentration. The LMVs in solution were filtered through a 0.45 μm pore polyethersulfone membrane to remove large particles and reduce the vesicle size. The solution was then warmed to 70˚C to ensure DSPC was in the liquid disordered phase and to facilitate extrusion. It was then extruded 11 times through a 100 nm pore polycarbonate

membrane filter (Whatman, Maidstone, UK) using a mini-extruder from Avanti Polar Lipids. A final solution of 1mM SUVs with a diameter of ~ 100 nm were obtained.

A diluted 0.2 mM SUV solution was used to form the lipid bilayer on the desired substrate. Substrates included mica, SiN_x wafers, untreated SiN_x windows, and pre-treated hydrophilic SiN_x windows, with all SiN_x materials purchased from Norcada (Edmonton, Alberta). To prepare the heterogeneous bilayer, the 0.2 mM SUV solution was pipetted on to the clean substrate and left to incubate for 1 hour at 70˚C. This temperature ensures that both lipids are in the liquid disordered phase, as the transition temperature for DSPC is 55˚C, while the transition temperature for DOPC is -17˚C (Avanti MSDS, 2015). The substrate containing the formed SLB was removed from the incubator. 5 mL of 70˚C 1x PBS was added to the petri dish containing the SiN_x window. The petri dish was carefully rinsed five times 3.5 mL aliquots of 70˚C PBS to remove excess vesicles. The SLB was then placed back into the incubator at 70˚C and cooled to 50˚C at a rate of 1˚C/10 minutes and then further cooled to room temperature at a rate of 5^0C/10 minutes.

The SLB films were imaged in 1x PBS using a Nikon Eclipse LV100N POL epifluorescence microscope (Nikon Instruments, Mississauga, ON, Canada) equipped with excitation and emission filters for Lissamine Rhodamine dye, and a 60X/0.85NA physiological objective. Images were acquired with a Retiga 2000R cooled CCD camera (QImaging, Surrey, BC, Canada) and recorded with the NIS-Elements AR software (Nikon, Tokyo, Japan). Fluorescence recovery after photobleaching (FRAP) tests were performed to test the mobility and integrity of the SLB on the substrate.

Dried SLBs were prepared for studies using STXM by first reducing the buffer salt concentration from 1x PBS to 0.75x, 0.5x, 0.3x, 0.1x PBS, rinsing thoroughly with five 3.5mL aliquots of the desired PBS concentration at each dilution. The buffer was ultimately removed and replaced with Mili-Q water. The bilayer film was re-imaged and then the Mili-Q water was removed by wicking off the excess with a Kimwipe™ and the sample was left to dry overnight in a sealed environment. The sample was then mounted on a STXM plate and imaged in transmission and fluorescence mode using the air objectives on the same microscope to locate possible areas of interest for STXM analysis.

2.e Difficulties Encountered Preparing Bilayers

The initial attempts to form SLBs were problematic, so an evaluation of the standard laboratory protocol [Zhu, 2015] was undertaken to determine which step(s) of the SLB generation procedure were compromising the ability to form bilayers. This section discusses the difficulties that arose when the standard laboratory procedure was followed. Figure 2.3 presents an initial result of a DOPC 50 / DSPC 50 SLB from Yujie Zhu on a mica substrate. This SLB sample does not contain the level of phase segregation that was observed using the optimized SLB formation procedure with a much slower cooling rate.
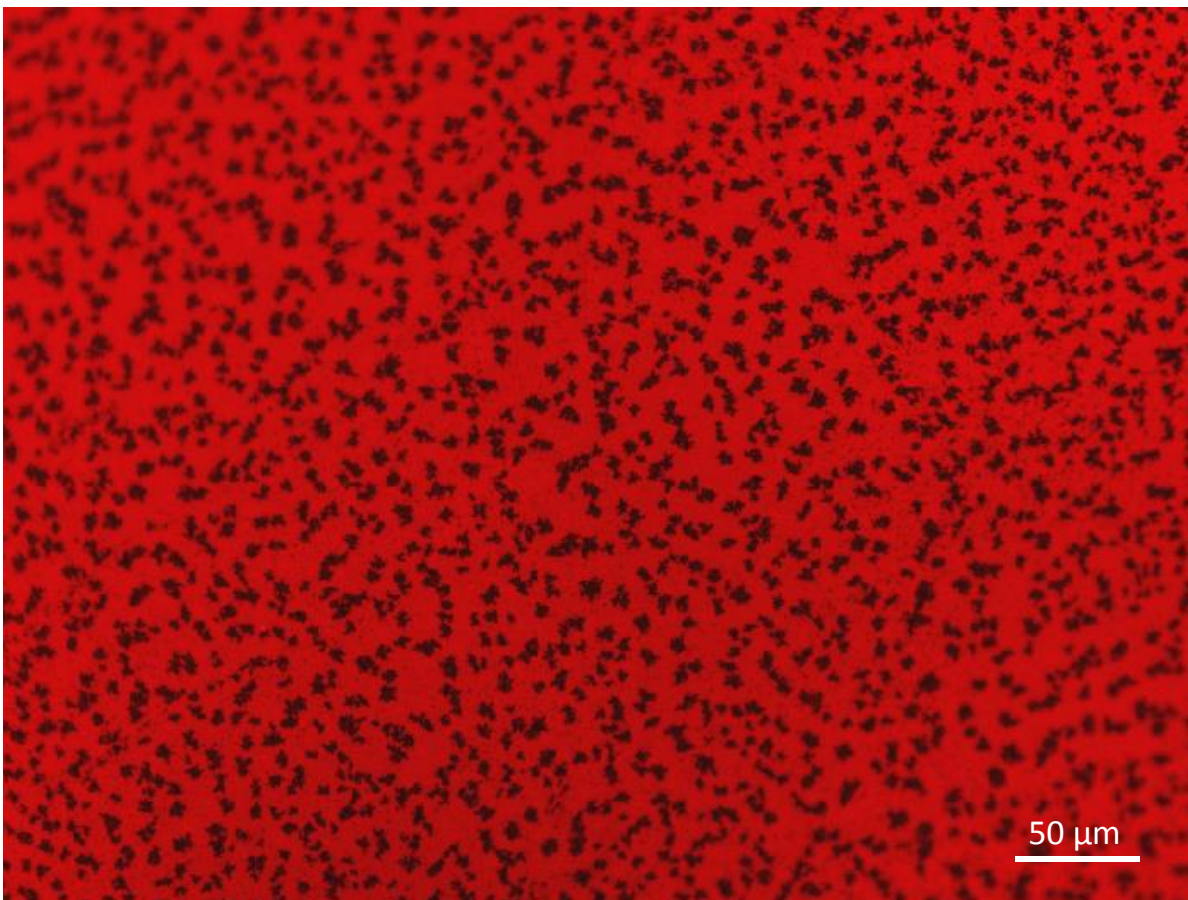
Figure 2.3. *An initial DOPC 50 / DSPC 50 SLB made on a mica support. Image courtesy of Yujie Zhu.*

Figure 2.4 presents FLM images of various concentrations of phase segregated lipid bilayers. The mobility of the bilayer in the preparation was confirmed through a FRAP test - the signal diffused laterally during both bleaching and recovery. The lipid concentration was varied sequentially to see the effect on the DSPC domain size that was produced. Although the domain size of DSPC did increase as its concentration increased, the morphology was unlike that reported in the literature [Adams, 2015]. This series of samples indicated that there may have been issues with either the substrate cleaning or the SLB solution preparation.

2.f Optimization of Bilayer Formation

The SLB preparation procedure was thoroughly analyzed to identify potential issues that would hamper the formation of an SLB. The three steps that required changes were: the cleaning of the glassware used to produce the lipid solutions, the washing of the bilayer films after incubation, and the rate at which the SLB was cooled after incubation. Forming heterogeneous lipid bilayers requires that multiple lipid species be mixed with a fluorescent dye in known ratios. Glass syringes (Hamilton Company Reno, Nevada) were used to measure the amount of each lipid and dye component. Initially, the glass syringe used for the lipid species was rinsed with HPLC grade chloroform three times in between changing lipid species. It was postulated that this amount of rinsing was insufficient to completely remove all of the previous lipid. The procedure was amended to perform five HPLC grade chloroform rinses between changing lipid species.

The procedure was also altered to include more rinses of the SLB with 1X PBS after it had been incubated to 70°C for 1 hour. The original procedure stated that three rinses with 4 mL aliquots

of buffer be used to wash the sample to remove any unfused small unilamellar vesicles (SUVs) from the substrate. The procedure was amended to increase the number of rinses to five, but to decrease the volume of buffer to 3.5 mL aliquots for each rinse, to ensure the SLB remained sufficiently hydrated and would not inadvertently dry, which would lead to the disruption of the bilayer.

The rate at which the SLB was allowed to cool in the original procedure was 2°C / min from 70°C to room temperature [Moran-Mirabal, 2007]. This procedure was followed for the samples shown in figure 2.4, but the DSPC domains did not phase segregate to a morphology shown in the literature. The amended procedure (section 2c) slowed the cooling rate to 1°C /10 min from 70°C to 50°C (just below the transition temperature of DSPC) and then from 50°C to room temperature at a rate of 5°C / 10 minutes. The changes to the original procedure from (Moran-Mirabal, 2007) culminating in the optimized procedure presented in section 2c significantly aided in the preparation of SLBs with a morphology similar to what has been presented in the literature [Adams, 2015]. An example of FLM of the same 3 mixtures showing the expected morphology, contrast and relative areas of DOPC (red) and DSPC (black) domains is shown in Figure 2.5.

DOPC 75 / DSPC 25

DOPC 50 / DSPC 50

DOPC 25 / DSPC 75
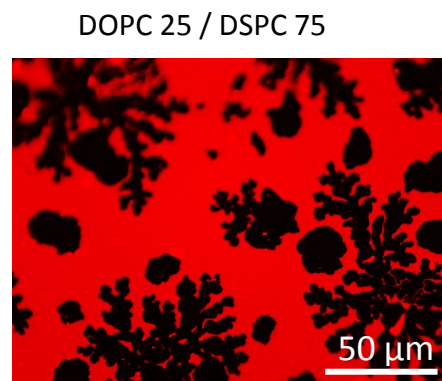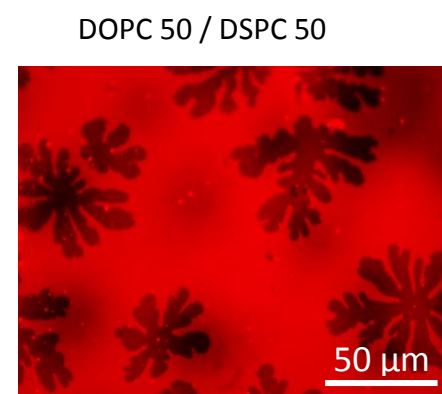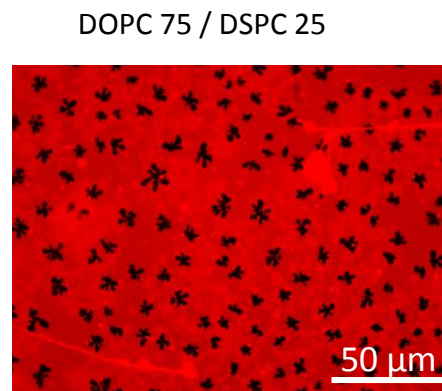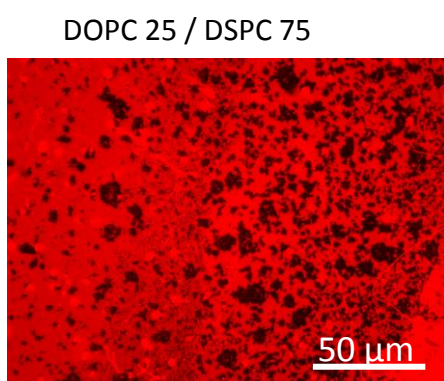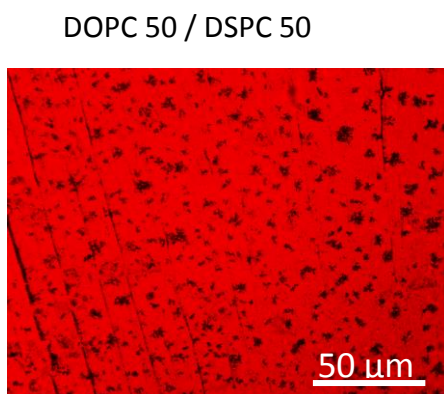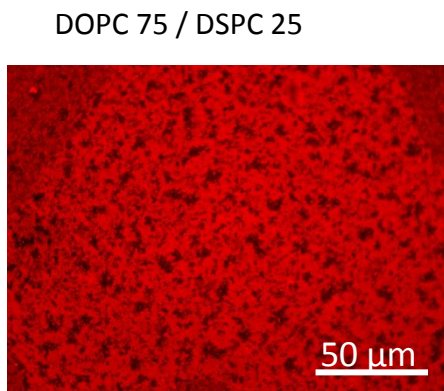
Figure 2.4. *DOPC/DSPC Lipid bilayers of various compositions with 0.1% DHPE: LR prepared on piranha cleaned SiO$_2$ wafers imaged in a 1x PBS solution.*

DOPC 75 / DSPC 25

DOPC 50 / DSPC 50

DOPC 25 / DSPC 75

Figure 2.5. *Lipid bilayers of various concentrations with 0.1% DHPE: LR prepared on mica and imaged in a 1X PBS solution, using the optimized procedure.*

2.g Two Dye Imaging of SLB

The DOPC and DSPC components of the bilayer were imaged by adding fluorescent dyes that are known to partition preferentially to each component. Lissamine Rhodamine B 1,2-dihexadecanoyl-sn-glycero-3-phosphoethanolamine, triethylammonium Salt (DHPE-LR) was used as the probe for DOPC and (1,1'-Dioctadecyl-3,3,3',3'-Tetramethylindocarbocyanine Perchlorate ('DiI'; DiIC$_{18}$(3))) was used as the fluorescent probe for DSPC. The excitation/emission wavelengths for DHPE: LR and DiI are 595/615nm and 549/565nm respectively [Sabnis, 2010]. Both dyes emit red, so DiI was used solely for confirmation of the presence of DSPC, as DiI is known to partition into the gel phase of DSPC [Konyakhina, 2013]. It was observed that DiI unexpectedly leached into the DOPC as well.

Samples containing DiI, such as those in Figure 2.6, were used to confirm the validity of the lipid preparation procedure. A single dye, DHPE: LR was used in the experiments where the areas occupied by the lipid components were calculated. The advantage with using a single dye was the contrast between the fluorescently tagged DOPC and the unlabeled DSPC was maximized, so the software was better able to distinguish between the two components within a sample.

DOPC 50 / DSPC 50
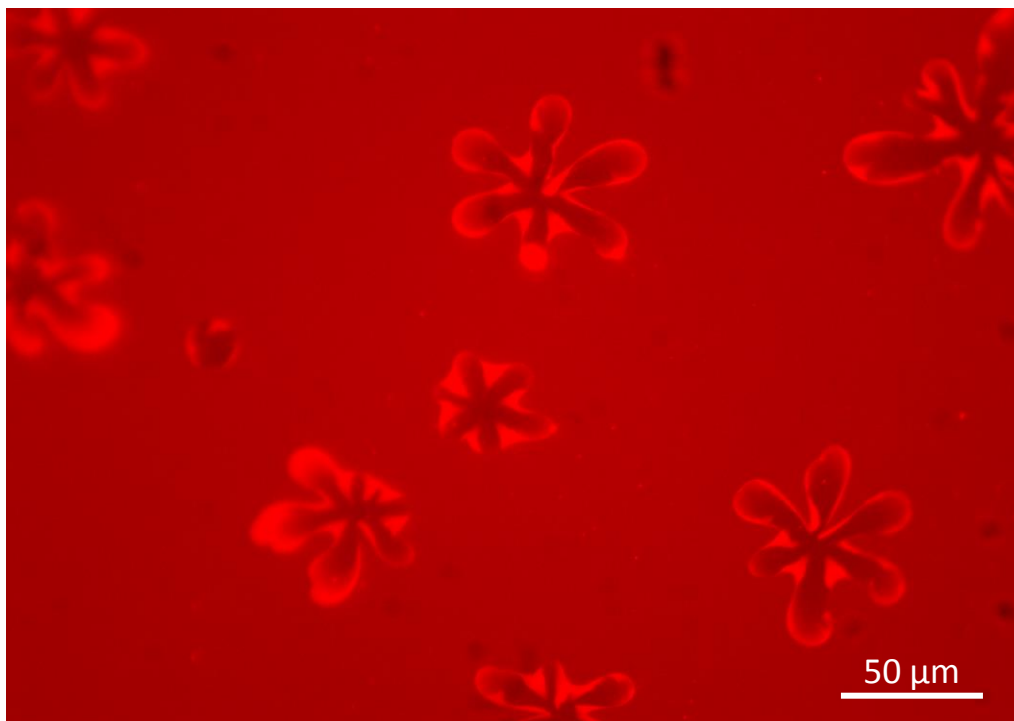
Figure 2.6. *A DOPC 50 / DSPC 50 SLB with 0.1% DiI on a mica substrate, imaged in solution with 1x PBS. The DiI partitioned into the DSPC domains and unexpectedly leached into the DOPC area.*

3. Methodologies – Lipid Reference Spectroscopy

3.a Content of this Chapter

This chapter presents and discusses the X-ray absorption spectra of four lipid compounds: 1,2-di-(9Z-octadecenoyl)-*sn*-glycero-3-phosphocholine (DOPC), 1,2-dioctadecanoyl-*sn*-glycero-3-phosphocholine (DSPC), and 1,2-di-(9Z-octadecenoyl)-3-trimethylammonium-propane (chloride salt) (DOTAP) and 1,2-dioleoyl-*sn*-glycero-3-phospho-L-serine (sodium salt) (DOPS) – see Figure 3.1 for the chemical structures of these species. The spectra were measured using STXM from multi-layer deposits solvent cast on silicon nitride window. These spectra can be used to identify, and quantitatively map the constituent lipids contained within a heterogeneous lipid bilayer film under both dry, and ultimately *in situ* hydrated conditions. The acquisition and interpretation of the C 1s, O 1s and N 1s spectra are discussed.

3.b Analysis of spectroscopic data

The optical transmission signal measured in STXM can be converted to absorbance or optical density (OD) using the Beer-Lambert Law (Equation 3.1),

$$OD = \log(\frac{I_0}{I}) \qquad\qquad (3.1)$$

where I_0 is the incident photon flux transmitted through a blank area on the SiN_x window, and I is the photon flux transmitted through an area where the sample is present. Regions with an OD > 2 were considered too thick to obtain valid data due to absorption saturation distortions when OD > 2 (Wan 2007). Once the beam was focused smaller area scans (10-50 µm) at 288.5 eV (the C 1s → π^* $_{C=O}$ peak of the carboxyl group of the lipid energy) on an area of suitable thickness were performed.

DOPC $C_{44}H_{84}NO_8P$
1,2-di-(9Z-octadecenoyl)-*sn*-glycero3-phosphocholine
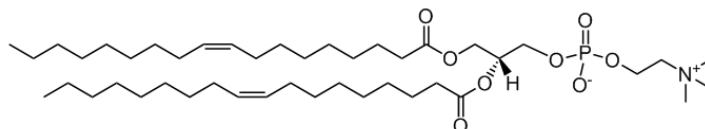
DSPC $C_{44}H_{88}NO_8P$
1,2-dioctadecanoyl-*sn*-glycero-3-phosphocholine
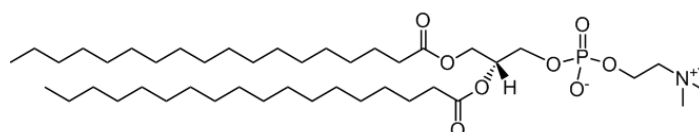
DOTAP $C_{42}H_{80}NO_4Cl$
1,2-di-(9Z-octadecenoyl)-3-trimethylammonium-propane Cl
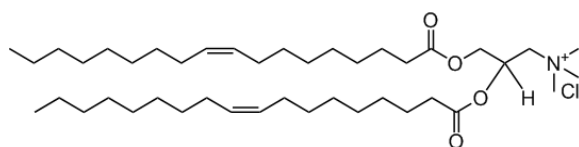
DOPS $C_{42}H_{77}NO_{10}PNa$
1,2-dioleoyl-*sn*-glycero-3-phospho-L-serine (sodium salt)
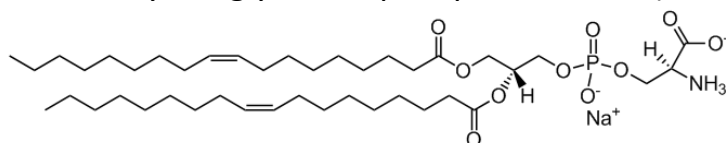
Figure 3.1. *Structures of lipids measured*

Lipid-specific maps were generated from images recorded at 280.0 and 288.5 eV. The transmission images of the pre-edge (280.0 eV) and on the peak of lipid absorption (288.5 eV) were converted to OD before subtraction. The C 1s stack maps were used to select an area for detailed study by a C 1s stack measured from 280 eV to either 326 or 340 eV. The energy step sizes were 0.10 eV from 284.0 to 289.0 eV, while larger energy steps (0.25-0.30 eV) were used for the C 1s pre and post edges. The dwell time used was either 1 or 2 ms, with pixel sizes ranging from 40-80 nm. The beam was defocused to between 150-200 nm, depending on the step size of the C 1s stack. It is critical to defocus the beam, so the damage to the lipid can be minimized.

NEXAFS stack alignment and analysis was performed using aXis 2000 [Hitchcock, 2014]. The stack data was read into aXis 2000 in transmission mode and aligned using the Jacobsen stack analyze alignment procedure. An appropriate area (either an internal blank area in a 1-region stack, or a second region in a 2-region stack measured simultaneously, or a carbon 1s point spectrum measured on a blank area of the SiN_x window) was used as an I_0. This allowed the data to be converted to OD. A mask of the areas containing the sample was created using the region of interest (ROI) selector on the average of all images. This ROI was then used to generate the OD spectrum of the specific lipid from the OD stack file.

The OD spectra were then converted to optical density per nanometer (OD1) spectra by taking the ratio of the OD spectra to the predicted elemental response. A constant was often used when generating OD1 spectra, to correct for changes in the response of the system in I and I_0 measurements made under different conditions. The elemental response is predicted from the molecular formula, the tabulated elemental X-ray absorption coefficients [Henke, 1993] and the

density of the material [Hitchcock 2012].   The density is an important factor to consider when generating OD1 spectra and will be discussed in detail below. Once the OD1 spectra were generated using aXis 2000, they were smoothed (if necessary) and plotted in SigmaPlot.

One must factor in the density of the lipid when generating the OD1 spectrum from the OD spectrum. If an incorrect density value is used, the scale of the OD1 spectrum will be off and result in inaccurate calculations of sample thickness when using the OD1 spectrum coupled with the OD spectrum of the sample of interest. The density of all of the lipids used in this experiment is reported by the manufacturer to be 1.480 g/cm^3 (Avanti Polar Lipids, MSDS). However, stearic acid (an 18 carbon carboxylic acid) is known to have a density of 0.9408 g/cm^3 at 20˚C [Rankin, 2009]. Additionally, the literature reports the specific volume of 18:1 phosphocholine (PC) lipids to be 0.9750 cm^3/g [Koenig, 2005]. Taking the inverse of the specific volume yields a density of 1.015 g/cm^3. Avanti Polar Lipids was contacted to elaborate on the density values they report in their respective MSDSs'. Avanti stated that the density reported is for a lipid solution in chloroform. The density of chloroform at 25˚C is known to be 1.489 g/cm^3 [Rankin, 2009], very close to the 1.480g/cm^3 reported by Avanti. Therefore if the value Avanti reports as the density was used to calculate the OD1 it would be for a chloroform lipid solution, not the true density of the lipid itself in water or dry conditions. The density of phosphocholines is known in the literature to be near 1.00 g/cm^3 [Koenig, 2005], so the OD1 spectra were generated using a density of 1.00 g/cm^3.

3.c Results of Lipid Spectroscopy using TEM grids and Chloroform Solvent

The purpose of generating valid lipid reference spectra is to be able to differentiate multiple lipids present within a bilayer. The first attempts at generating lipid spectra were made using solvent casting the relevant lipid as a lipid agglomeration onto a formvar coated TEM grid. Figure 3.2 plots (a) spectra and (b) spatial mapping of 2-components found in a sample of DOPC (JDW030). The DOPC sample (JDW030), which should be pure, shows two regions with distinct spectral features (indicated by the red and blue areas).   L1, 1-palmitoyl-2-hydroxy-sn-glycero-3-phosphocholine and L2 (1-arachidoyl-2-hydroxy-*sn*-glycero-3-phosphocholine) are previously recorded lipid reference spectra [Lawrence, 2003].

The carboxyl (C=O) peak that appears at 288.5 eV (indicated by the solid black line) on the L1 and L2 spectra is shifted compared to the first peak in the JDW030 sample that was measured. The 288.5 eV peak is well known in the literature to indicate a C 1s(C=O) 1s $\rightarrow$ π^*_{COO} transition [Hitchcock, 1994, Rühl 1991,Benzerara, 2004, Cody 1998, Lehmann 2005, Schumacher 2005]. Therefore, it was concluded that the spectroscopic results for the sample JDW030 did not conform to what was expected and was invalid.

a

b
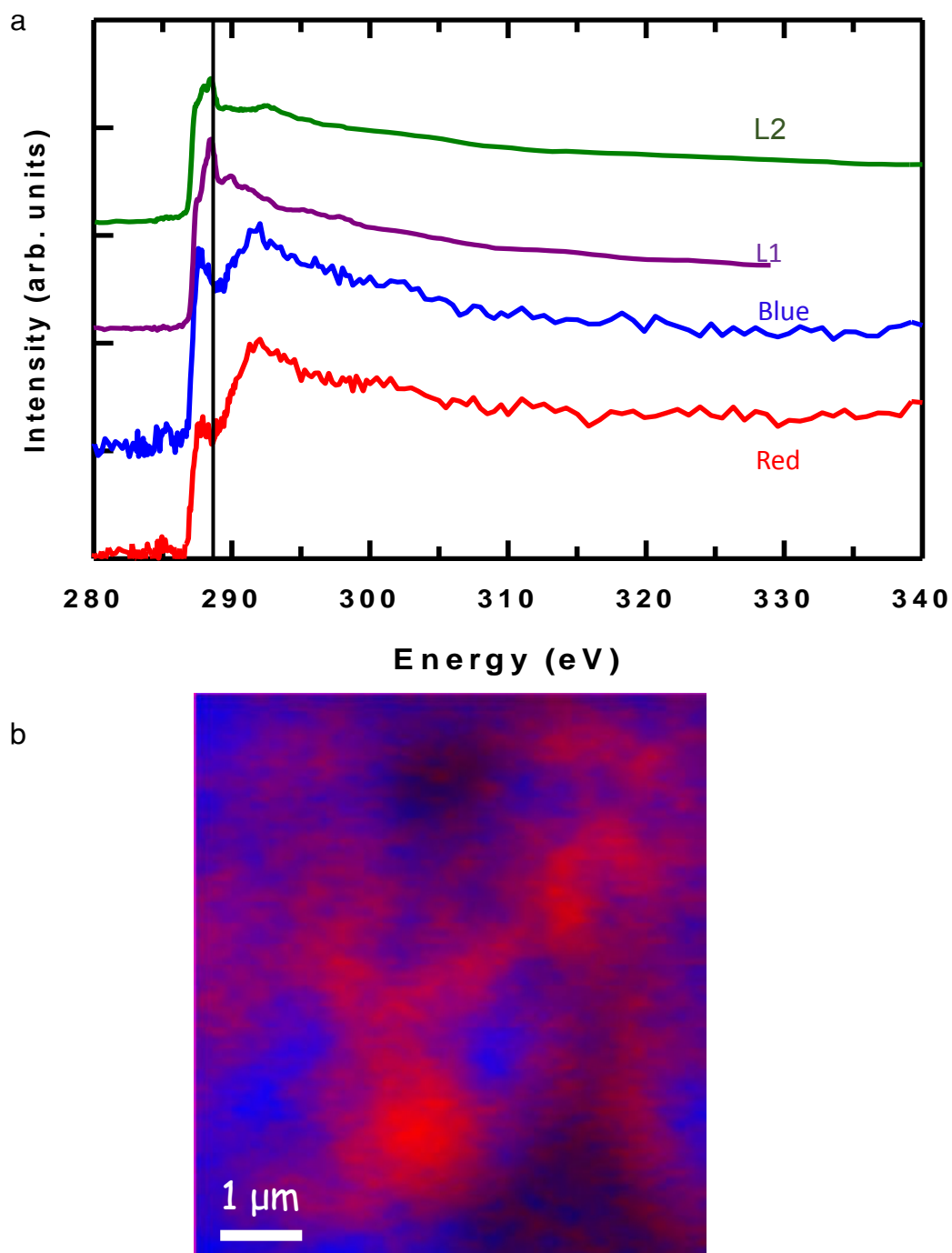
Figure 3.2. *A DOPC lipid sample (JDW030) solvent cast from chloroform. (ALS5.3.2.2, Sep 2014). a. spectra from two component stack fit. b red/blue display of the two*

Chloroform was used as the solvent from which JDW030 was dropcast onto a formvar-coated TEM grid. Further attempts at generating valid reference spectroscopy were tried using chloroform as the solvent and TEM grids as the substrate, but similar results were obtained. The STXM literature has shown amorphous carbon has accounted for impurities within sample (Najafi, 2008). A previous graduate student in the Hitchcock lab, Dr. Cynthia Morin, experienced difficulties with sample impurities with her protein on patterned polymer surfaces studies (Morin, 2004). The impurities she encountered were similar to the ones in this project, consisting of both solvent and annealing procedure impurities (Morin, 2004). The use of toluene as a solvent has previously been shown to lead to inhomogeneous distributions of component species in polymer blends (Walheim, 1997), such as the ones Dr. Morin used for her studies. It was postulated that the chloroform-lipid solution which was used to dropcast the lipid onto the TEM grid may have inadvertently dissolved some of the 3M tape used to secure the TEM grid to the STXM plate and caused amorphous carbon deposits on the grid itself. This may be the source of the impurities observed within the JDW030 sample.

As it was speculated that casting the lipid from chloroform may have been the cause of impurities, the solvent used to cast the sample was switched to water (as described in section 3b). An aqueous solution was used for two reasons: a) it was thought that the impurities present from the chloroform solution could be avoided, and b) future experiments would involve the preparation of a lipid bilayer under aqueous conditions, so a spectrum generated under aqueous conditions would be more representative of future experiments.

Figure 3.3, presents the spectrum of a DOPC sample (JDW040). The spectrum in red is that of DOPC while the spectrum in black is the spectrum of potassium ions in a biofilm [Neu, 2010].

Clearly, potassium ions were present in this DOPC sample. Referring to the structure of DOPC (Figure 3.1), DOPC is zwitterionic, meaning that there should not be potassium present as a counter ion. The manufacturer, Avanti Polar Lipids was contacted to ask if potassium was present in their DOPC lipid. They responded that they do *not* add potassium to DOPC because it is zwitterionic, but they do not assay for potassium impurities either.

Generating valid lipid reference spectra continued to be problematic until spring 2015. The sample preparation protocol was changed to the procedure reported in chapter 2. The substrates used were changed from TEM grids to SiN_x windows and more glassware cleaning steps were added. Impurities were present in four attempts at generating a DSPC C 1s reference spectrum (see figure 3.4). These impurity issues were worked through and ultimately valid C 1s, N 1s, and O 1s reference spectra were generated for DOPC, DSPC and DOTAP. In addition a valid C1s spectra was generated for DOPS.
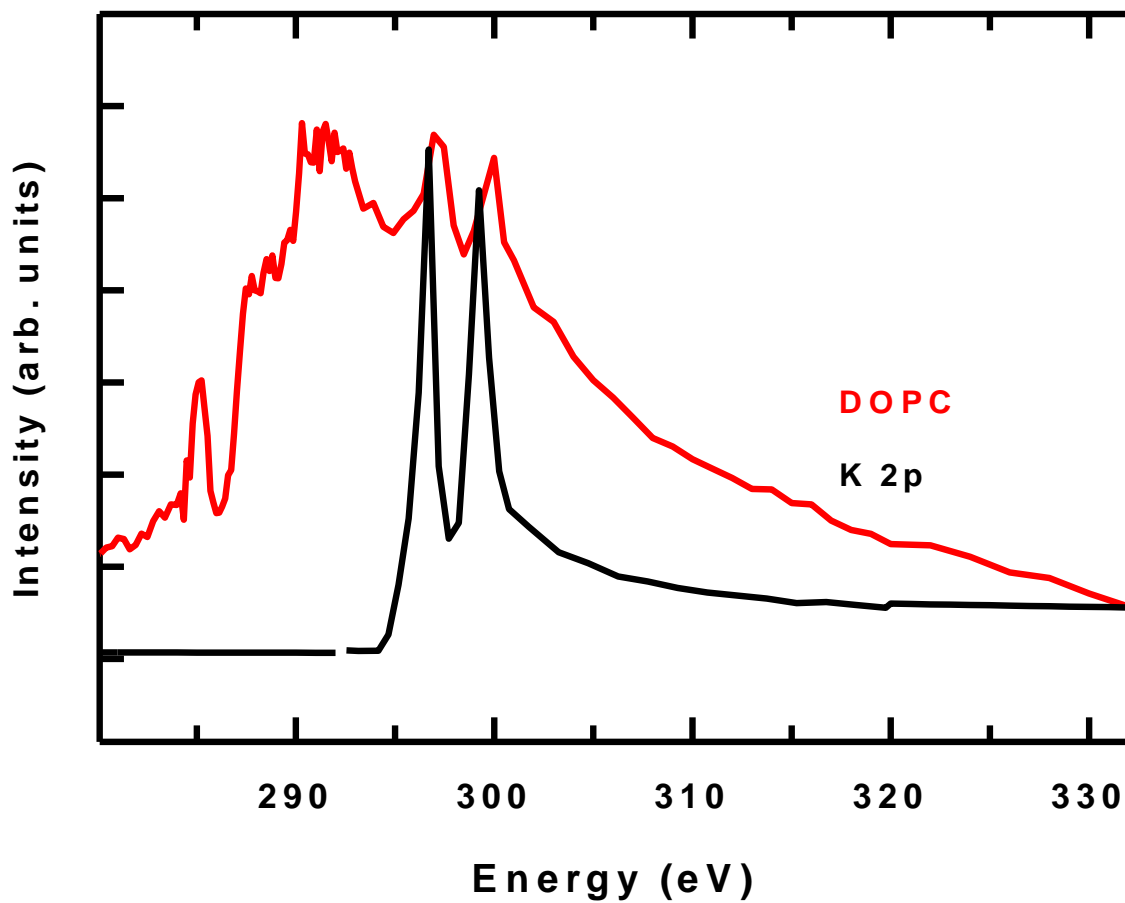
Figure 3.3. *STXM absorbance spectrum of DOPC sample cast from water onto TEM grids (reference number JDW040) analyzed at the CLS in February 2015. The absorbance spectrum of potassium shows impurities in this DOPC sample.*
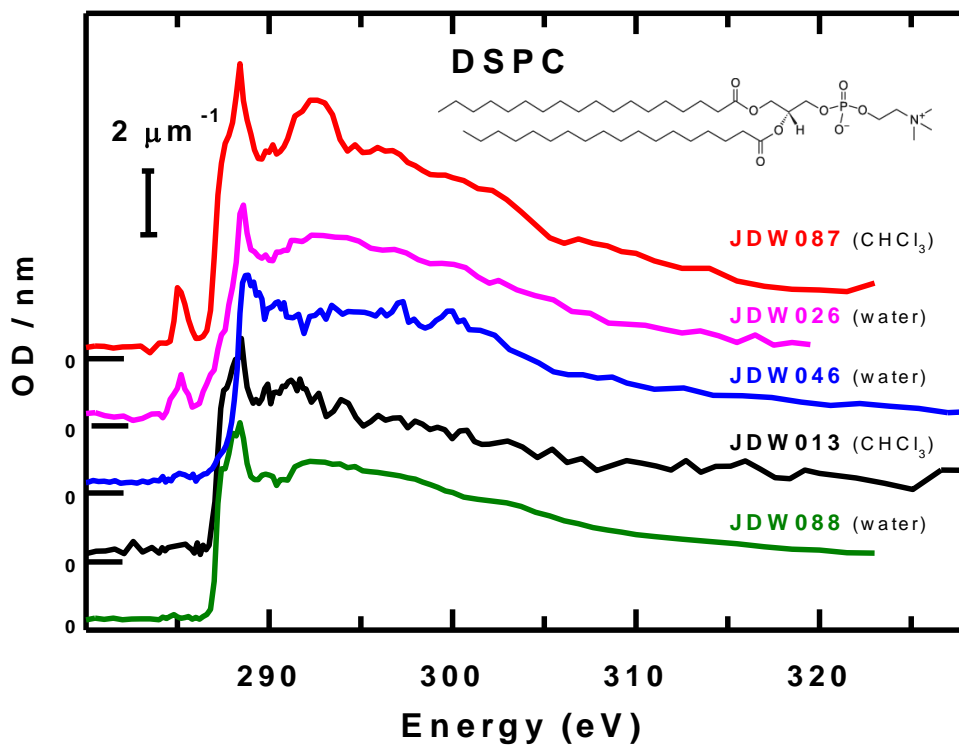
Figure 3.4. STXM C 1s spectra of 5 different samples of DSPC, prepared on formavar-coated TEM grids by solvent casting and measured at different times. Only the JDW088 sample cast from aqueous solvent is considered to be free of impurity contributions, with that decision based on its similarity to C 1s spectra of other the lipids which are considered reliable. A detailed discussion of possible causes of incorrect results in the other cases is presented in the text.

3.d Results of Lipid Spectroscopy using SiN$_x$ Windows and Aqueous Solutions

Figure 3.5a presents the final, optimized C 1s spectra of DOPC, DSPC and DOTAP on an OD1

scale. The C=C 1s→π* transition occurs at 285.1 eV for isolated C=C bonds, as in DOPC and

DOTAP [Hitchcock, 1994, Rühl 1991,Benzerara, 2004, Cody 1998, Lehmann 2005, Schumacher

2005] and is responsible for the 285.1 eV peaks on the spectra of the unsaturated lipids DOPC

and DOTAP. The C 1s$_{(C=O)}$ →π* carbonyl transition occurs between 287.7 – 288.6 eV [Benzerara,

2004, Cody 1998, Lehmann 2005, Schumacher 2005]. The sharp peak present in all three lipids

at 288.5 eV is attributed to the C 1s →π*$_{C=O}$ transition in the carboxylate group [Urquhart,

2002].

The energies and proposed assignments for the spectral features for Figure 3.5b are listed in

table 3.1. The amount of nitrogen in the lipids is extremely small but the presence of this weak

signal, with a very similar spectral shape in each of the lipid species, consistent with the

presence of a quaternary ammonium group in each molecule, is a satisfying confirmation of

molecular identity. The 401.3 eV peak is associated with the N 1s → 3s (Rydberg) transition

[Gordon, 2003]. The broad peak at 406.7 eV is assigned as N 1s → σ*C-N as shown previously in

[Gordon, 2003].   The energies and proposed assignments for the spectral features in Figure

3.5c. are listed in Table 3.1. The spectra have been scaled to match the predicted elemental

response of 1 nm at ρ = 1.0 g/cm^3. While the amount of oxygen in lipids is relatively small, the

characteristic O 1s → π* transition at 532.1 eV from the carboxylate in the polar head group is

a useful confirmation of the correct identification of a lipid. The peak present at 535.3 eV is the

O 1s(OH) → π*(COOH) transition [Gordon, 2003]. The large, broad peak at 540 eV is due to the

O 1s $_{(O-C)}$ →σ*O-C transition [Gordon, 2003].
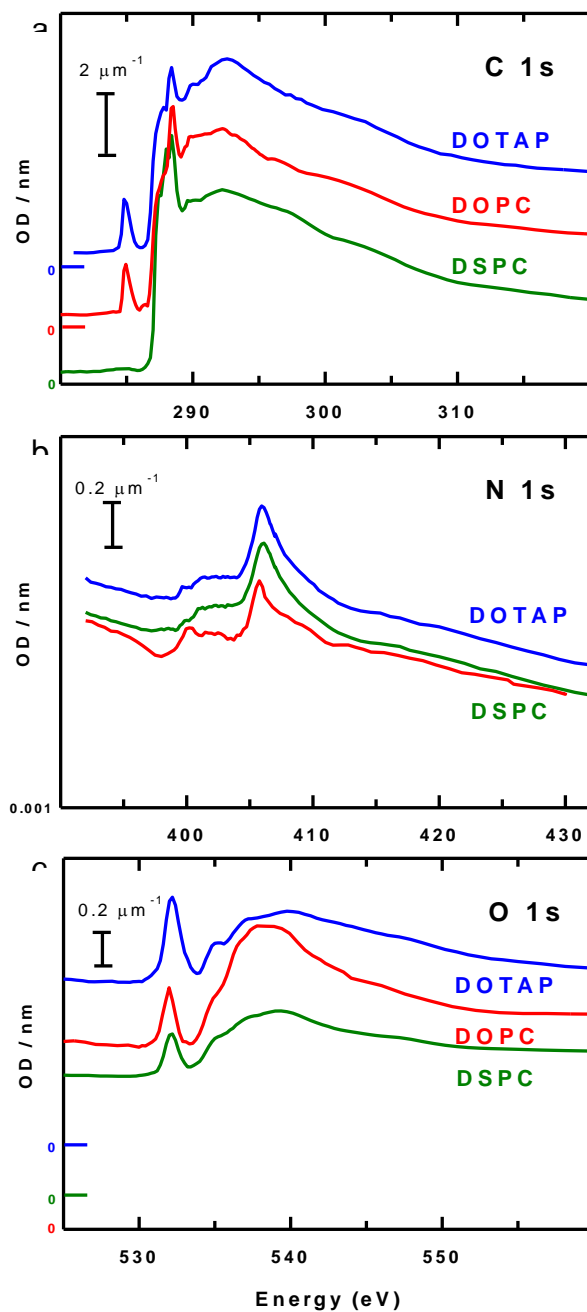
Figure 3.5a *C 1s spectra of DOPC, DSPC and DOTAP. The spectra are presented with intensities on the OD1 scale - i.e. the relative spectra have been scaled to match the predicted elemental response of 1 nm at $\rho = 1.0$ g.cm^{-3}. Offsets are added for clarity - the zero of each spectrum is indicated. Energies and proposed assignments for the spectral features are listed in* table 3.1.

Figure 3.5b. *presents the N 1s spectra of DOPC, DSPC and DOTAP on an OD1 intensity scale.*

Figure 3.5c. *presents the O 1s spectra of DOTAP, DOPC, and DSPC on OD1 intensity scales, with offsets for clarity.*

Table 3.1. *Proposed assignments for features in the C 1s, N 1s, and O 1s spectra of DOPC, DSPC, and DOTAP.*

C 1s

#		Energy (eV)			Proposed Assignments		
	DSPC	DOPC	DOTAP		C=C	CH$_2$	CO$_2$
1.	-	284.9	285.0		$\pi^*_{C=C}$		
2.	287.6	287.6	287.6		-	σ^*_{C-H}	
3.	288.39	288.43	288.48				$\pi^*_{C=O}$
4.	289.9	289.9	289.9				
5.	292.3	292.3	292.6			σ^*_{C-C}	
6.	301.8	301.8	301.8				$\sigma^*_{C=O}$

N 1s

#		Energy (eV)			Proposed Assignments
	DSPC	DOPC	DOTAP		NMe$_3$
1.	406.7	406.8	406.8		σ^*_{C-N}

O 1s

#		Energy (eV)			Proposed Assignments	
	DSPC	DOPC	DOTAP		C=<u>O</u>	C(=O)-<u>O</u>
1.	532.1	532.1	532.1		$\pi^*_{(COOH)}$	
2.	535.3	535.3	535.3			$\pi^*_{C(=O)-O}$
3.	540	539	540			σ^*_{O-C}

3.e Discussion of the reliability of the lipid reference spectra

The proper application of STXM spectroscopy for the chemical identification and spatial mapping of lipid species in a bilayer relies on the existence of previously generated, impurity free, valid, X-ray absorption spectra of the pure species. Therefore, a systematic assessment of lipid spectra obtained through different sample preparation approaches was conducted to ensure that the lipid reference spectra obtained were reliable and free of signal from impurities. The simplest way to differentiate between saturated (e.g. DSPC) and unsaturated lipid species (e.g. DOPC, DOTAP) is by using the C 1s absorption spectrum, where the C $1s_{(C=C)}$ →π* C=C transition at 285.1 eV occurs in unsaturated but not in saturated lipids [Benzerara, 2004, Cody 1998, Lehmann 2005, Schumacher 2005]. This peak was expected to appear in the C 1s spectra of unsaturated lipids, but not in that of DSPC since its carbon chain consists of only aliphatic C-H bonds. Thus, deducing the correct spectrum of DSPC made use of the absence of the 285.1 eV peak. From Figure 3.4, it can be seen that JDW087 and JDW026, DSPC samples drop-cast from water and chloroform, both contain 285.1 eV peaks. These spectra are not consistent with a saturated lipid and suggest the presence of contaminants that contain unsaturated C=C bonds.

Similarly, JDW046 and JDW013 had shifted energy peaks for the C 1s (C=O) carbonyl transition that is expected occur at 288.5 ±0.1 eV [Benzerara, 2004, Cody 1998, Lehmann 2005, Schumacher 2005]. The C 1s spectrum of JDW046 also presented absorption peaks at 297.0 and 299.0 eV, indicative of the presence of potassium. According to the supplier potassium should not be present in any of the lipids studied, which implied that the potassium peaks observed arose from contaminants introduced during the sample preparation. As a comparison, a true

reference spectrum for DSPC (that of sample JDW088) is presented in Figure 3.5, which shows the expected absorbance profile and absence of impurities.

The generation of valid reference spectra required overcoming significant contributions from impurities, and improving the experimental protocol used for lipid sample preparation. For example, use of chloroform as a solvent for lipid sample casting inevitably led to the appearance of impurities in the spectroscopy of the sample. These impurities could arise from the solvent dissolving small amounts of adhesive contained in the mounting tape used to secure the SiN_x windows onto the STXM sample plate or from any plastic material containing chloroform soluble components that the chloroform comes in contact with. The adhesive could migrate onto the SiN_x window, contaminating the sample and causing the spectra to contain different features than those expected.

However, in two other DSPC samples (JDW026 and JDW046), where DSPC was dropcast from water, there were still impurities, as evidenced by the unexpected presence of the 285.1 eV C $1s_{(C=C)}$ →π* C=C transition and the energy shift for the C $1s_{(C=O)}$ →π* C=O transition at 288.5 eV. The impurities contained in these samples may have originated from organic contaminants not being entirely removed by the piranha cleaning processing of the glassware used in the experiment. It has been shown in the STXM literature that amorphous carbon has been present in samples as impurities, which may account for the impurities observed on four of the DSPC samples in this experiment [Najafi, 2008]. The C 1s spectrum of JDW088 contains all the expected transitions that have been previously reported in the literature, without the obvious indications of impurities that marred the other attempts at generating the C 1s DSPC spectrum. The C 1s spectra of all three lipids (Figure 3.5) are consistent with what is expected.

Figure 3.4 also shows all the spectroscopic issues that arose with regard to sample impurities during preparation. Since the impurity problems have been worked through and the spectra conform to known transitions reported in the literature, it can be concluded with reasonable certainty that these lipid spectra are valid.

4. Analysis of Bilayer Compositions

4.a Content of this Chapter

This chapter outlines the analysis of lipid bilayer phase segregation using Image J and aXis 2000 software. This analysis helped to provide confirmation of valid SLBs. A video showing the phase segregation of DSPC into domains is provided as external media for this thesis and can be found at http://unicorn.mcmaster.ca/highlights/FM-lipid-bilayers/FM-lipid-bilayers.html.

4.b Bilayer Composition Determined from Area Determinations

Image J was used to calculate the areas of each lipid within a sample. A fluorescence image of a sample was taken under hydrated conditions in 1x PBS and a mask of the DSPC domains was generated using Image J. A mask of the area containing unfused vesicles was also generated, so that area could be subtracted because it did not contribute to the bilayer area.

The IsoData algorithm was used to generate the DSPC domain mask (Figure 4.1). IsoData is an iterative procedure that divides the fluorescence image into a background and object using the initial threshold, where Threshold = (average background + average objects)/2 [Ridler, 1978]. The averages of the pixels at or below the threshold and above the threshold are calculated and an average of those two values is calculated and the threshold is incremented, repeating the process until the threshold is greater than the composite average [Ridler, 1978]. The number of pixels comprising the DSPC domains was subtracted from the total number of pixels in the image and this number of pixels was divided by the total, to give the corresponding percentages of the area accounting for each lipid. This process was done for a series of DOPC/DSPC concentrations with

the results presented in **Table 4.1**, where it is shown that the size of the DSPC domains and their total area was dependent of the concentration of DSPC.

Figure 4.2 presents the DOPC / DSPC area results graphically. It is known that unsaturated and saturated lipids occupy different areas. This was accounted for by applying a correction factor. DOPC is known to occupy an area of 0.724 ± 0.005 nm^2 [Kučerka, 2006] whereas DSPC is known to occupy an area of 0.638 ± 0.013 nm^2 [Kučerka, 2011] under hydrated conditions. This area difference of approximately 15% was accounted for in the DOPC and DSPC areas reported in Table 4.1 and Figure 4.2.

a   Fluorescence

b   DSPC domain mask

c   Unfused vesicles
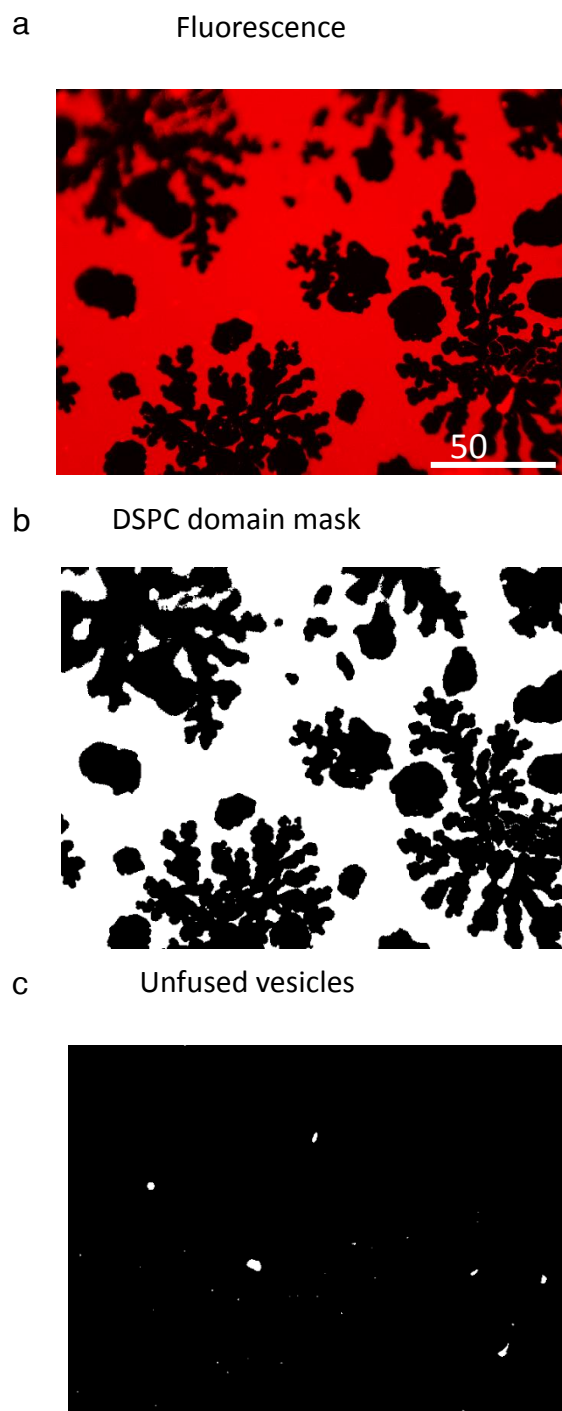
Figure 4.1. *A DOPC 25 / DSPC 75 SLB with 0.1% DHPE:LR on a mica substrate, imaged in solution with 1X PBS.*

Table 4.1. *Calculated areas of DOPC and DSPC in a DOPC 75 / DSPC 25 bilayer sample.*[1]

DOPC 75- DSPC 25 0.2mM Mica
Wet

Image	Total Area	% Area DOPC Corrected (Uncorrected)	% Area DSPC Corrected (Uncorrected)
Area A.tif	43842	85.2 (87.1)	14.8 (12.9)
Area B.tif	42918	85.5 (87.4)	14.5 (12.6)
Area C.tif	47779	83.8 (85.9)	16.2 (14.1)
Area D.tif	44645	84.9 (86.9)	15.1 (13.1)
Area E BB.tif	56702	80.8 (83.3)	19.2 (16.7)
	AVERAGE	84.0 ±1.8	16.0 ±1.8

Table 4.2. *Areas of DSPC for three different DOPC/DSPC bilayer samples.*

Input % DSPC	Corrected Measured Mean % DSPC	Standard Deviation	95% Confidence Interval
25	17	1.9	1.7
50	33	9.0	5.9
75	53	3.3	1.9
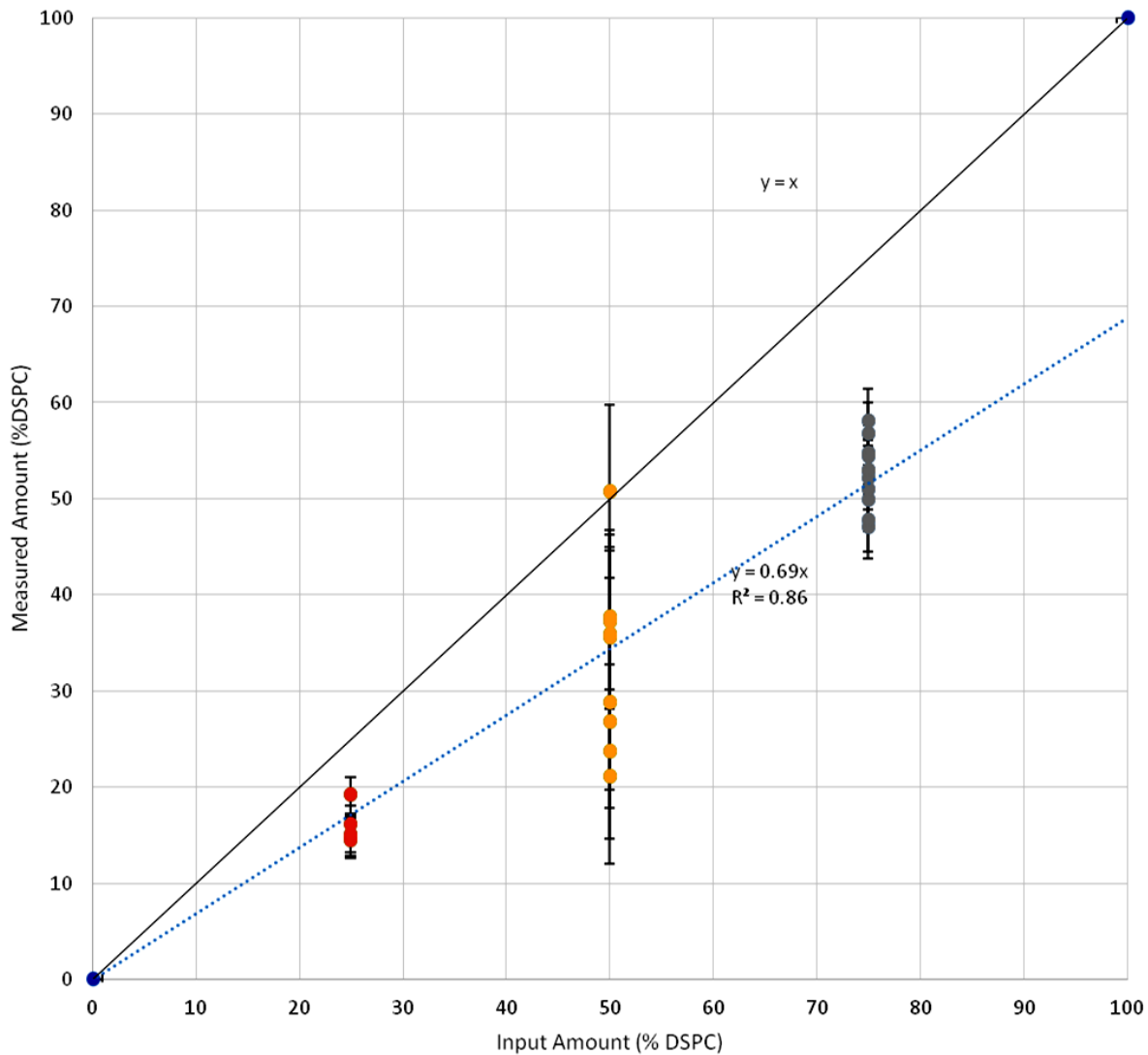
Figure 4.2. *Measured amount of DSPC in various SLB concentrations plotted against the input concentration of DSPC. The error bars represent the standard deviation. The plot y=x is shown for comparison.*

Although the trends are linear (as shown by the R^2 value of 0.86), the trend line does not have a

unit slope and the % area (of DSPC) in each of the SLB concentrations (units are in mol %) in the

samples: DOPC 75 / DSPC 25, DOPC 50 / DSPC 50, and DOPC 25 / DSPC 75 ratios does not

present the exact composition used in making the SLBs. The areas containing the SLB were

imaged on a mica substrate, where the bilayer was sometimes non-uniformly distributed across

the surface. This may account for the discrepancy between the observed component areas and

the calculated component areas. Additionally, there is never perfect phase segregation of the

lipids, as they were not cooled for an infinitely slow time and phase segregation is imperfect.

This experiment further validated the SLB formation procedure and showed the ability to

control the size of the DSPC domains by varying the concentration of the component lipids and

also control the domain size by increasing the annealing time using a slower cooling rate.

4.c Video of Bilayer Formation

The video appended to this thesis (found at http://unicorn.mcmaster.ca/highlights/FM-lipid-

bilayers/FM-lipid-bilayers.html) shows the segregation of DSPC from DOPC and the formation

of isolated DSPC domains. This occurs when the SLB is cooled to below the transition

temperature of DSPC (55˚C) [Avanti MSDS, 2015] and changes phases to the gel phase. This

sample in the video is a DOPC 25/ DSPC 75 / 0.1 DHPE: LR sample on a mica substrate, imaged

under hydrated conditions in 1x PBS. The video has been sped up eight times, so the formation

of phase segregated domains can be clearly seen.
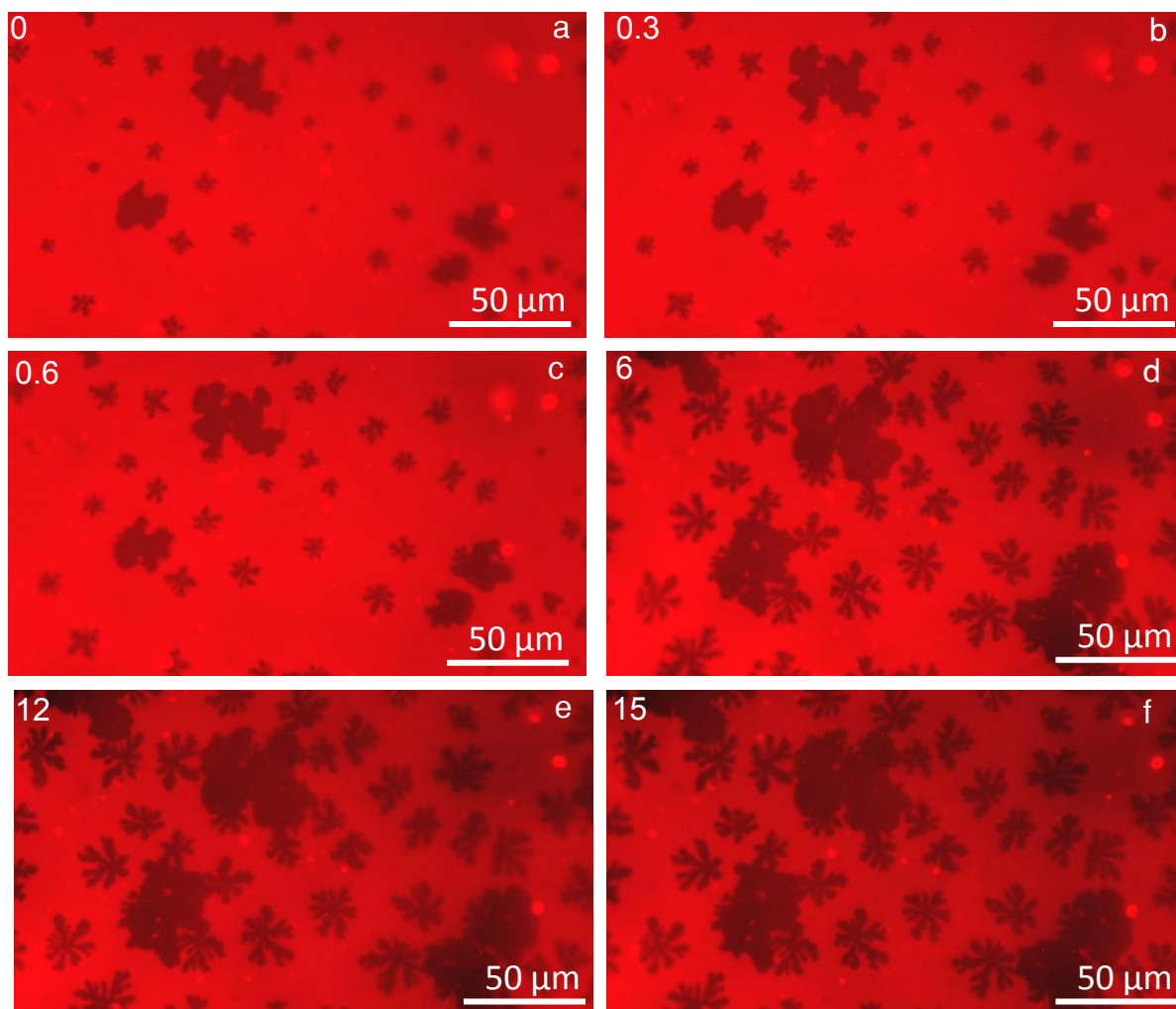
Figure 4.3. *Screenshots of the DOPC 25 / DSPC 75 lipid bilayer video at the indicated time intervals, while cooling through the DSPC transition temperature of 55˚C.*

5. Optimization of static lipid bilayer wet cells

5.a Content of this Chapter

Chapter 5 outlines my attempts at creating static wet cells using both hydrophobic and hydrophilic SiN_x windows. The valid reference spectra that were generated in Chapter 3 allow for the analysis of a mixture of separate unsaturated/saturated lipids based on C 1s spectromicroscopy found in Chapter 5.c. Through comparison to fluorescence optical microscopy, it is demonstrated how STXM measurements combined with the C 1s reference spectra of DOPC and DSPC can be used to map these two lipid species in a thin bilayer film.

5.b Initial Attempts using Hydrophobic SiN_x Windows

This section presents results of a STXM analysis of a multicomponent lipid bilayer under dry conditions. Static wet cells were created to keep the bilayer hydrated and provide a mimic for a naturally occurring hydrated environment of lipid bilayer membranes. The first attempts at creating a static wet cell made use of Norcada SiN_x windows with frame dimensions of 5 x 5 mm, frame thickness of 200 μm, window area is 0.5 x 0.5 mm and a 100 nm thick SiN_x window membrane.

a   DOPC 75 / DSPC 25

b   DOPC 50 / DSPC 50

c   DOPC 25 / DSPC 75
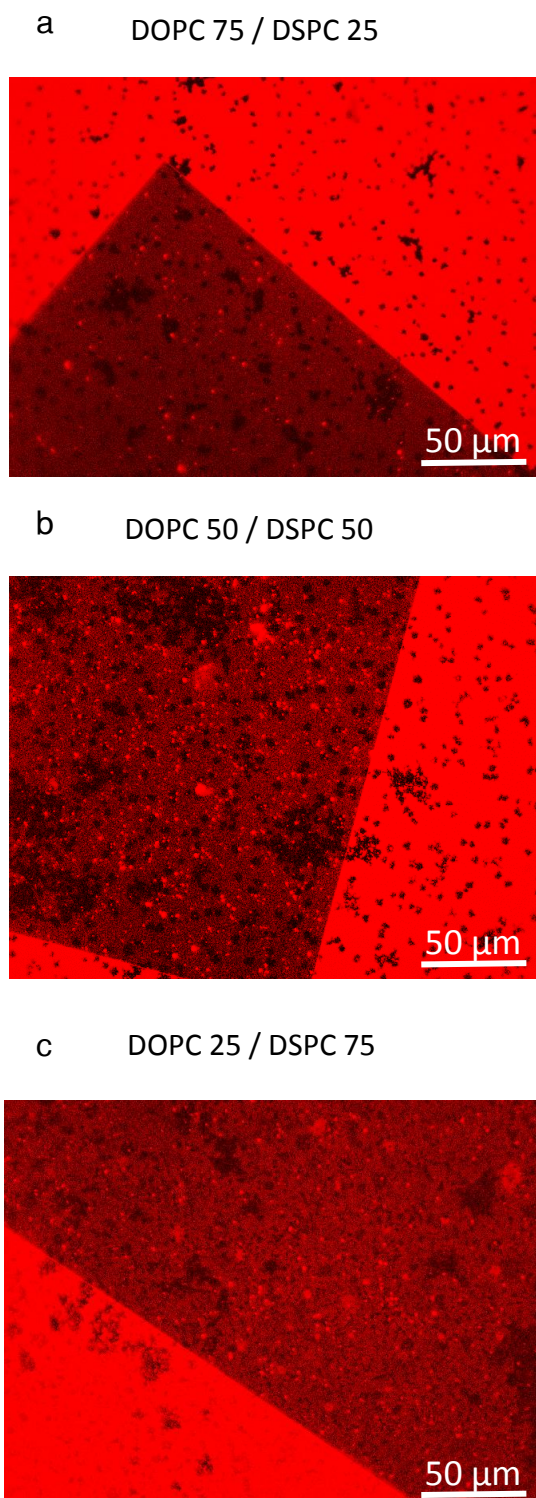
Figure 5.1. *The formation of SLBs in three ratios with 0.1% DHPE:LR on piranha cleaned / plasma cleaned SiN$_x$ RW1 windows from Norcada.*

The SLBs were formed using the procedure outlined in chapter 2. The morphology of the bilayer is dependent on the hydrophilicity and cleanliness of the substrate. The morphology should be similar to Figure 4.2, where different concentrations allow for varying domain sizes of DSPC. However, this was not observed on any Norcada 0.5mm x 0.5mm SiN$_x$ windows, even after the piranha and plasma cleaning steps outlined above.

The first static wet cells were constructed using the Norcada 0.5 x 0.5 mm SiN$_x$ windows. Once the bilayer was formed on a window, the window containing the SLB was kept hydrated and placed on double-sided tape attached to a STXM plate. A blank, piranha/plasma cleaned window was overlapped with the window already mounted on the STXM plate. By mounting the window membranes in a direction facing each other (Figure 5.2), the thickness of the water layer was able to be controlled at the desired level (~1-2 µm), suitable for soft X-rays to transmit through the water layer. The ideal water layer is several hundred nanometers thick. The thickness of water layers can be estimated by looking at the interference fringes using an optical microscope. A 5-minute curable epoxy was then used to create a seal around the two SiN$_x$ sandwiched windows.

Additional means were explored to control the thickness of the water layer, including: marking the frame of the window with a Sharpie felt tip pen, adhering polystyrene beads of 1 µm thickness to the window and frame areas, and most effectively, coating the surface of the frame with a controlled thickness of Parylene-C.

The JDW006 static wet cell sample gave useful feedback on both the benefits and limitations of the static wet cell samples. The positive result of JDW006 was the use of a 100 nm Parylene-C coating on each frame to control the thickness of the water layer, limiting the amount of water

in the sealed sample, thus permitting soft X-rays to pass through the sample and be detected. Parylene-C was used with the flow cell part of this project to both control the thickness and bond SiN_x chips and will be explained in greater depth in Chapter 6.

JDW006 made use of a 5-minute curable epoxy from 3M. The relatively long cure time of the epoxy allowed for inadvertent leaching of the epoxy into the wet cell and contaminated the sample. This is clearly visible in the RGB component map in Figure 5.3, where the epoxy (green) leached through the entire sample. Radiation damage was also observed from the water present in the sample being hydrolyzed due to the soft X-rays. Plotting the lipid spectra from the wet cell (blue) against a lipid reference spectra (L1, 1-Palmitoyl-2-Hydroxy-sn-Glycero-3-Phosphocholine) [Lawrence, 2003] suggests that there is a lipid present in the wet cell, but that its spectrum is incorrect because it does not exhibit a π* peak at 285.1 eV which is expected for unsaturated lipids (DOPC) and unsaturated carbon containing compounds generally.
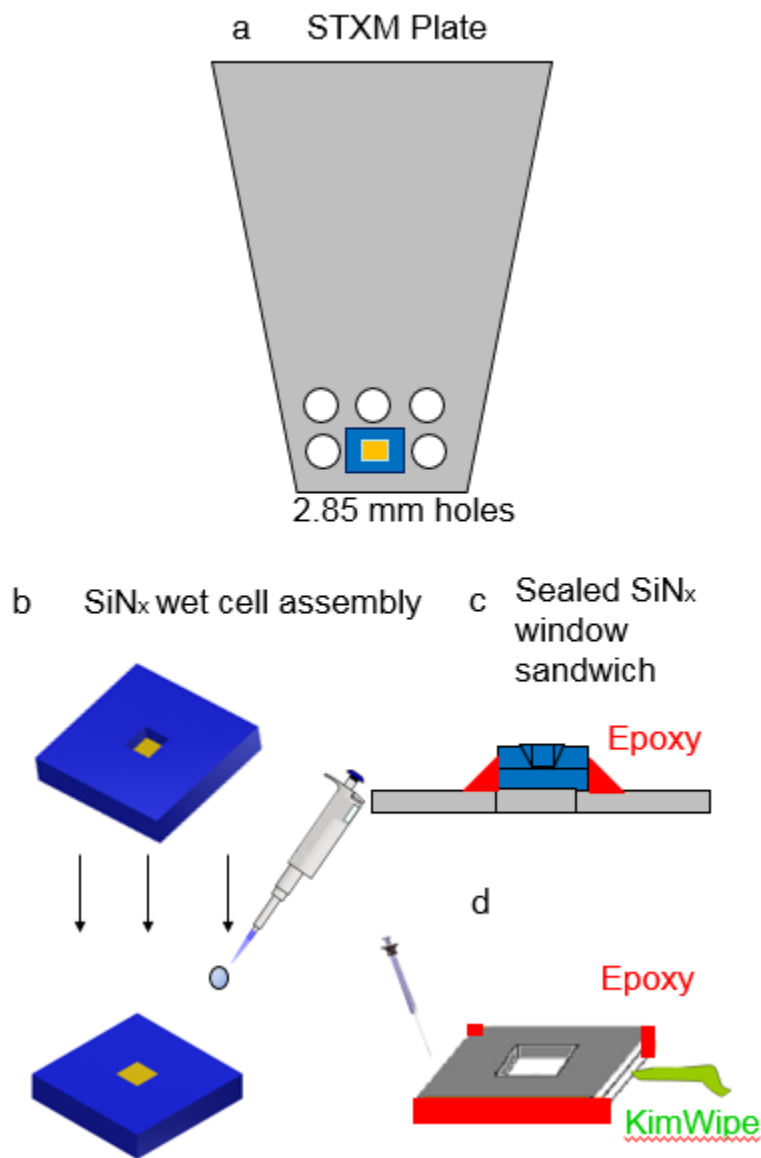
Figure 5.2. *The construction of a static wet cell using SiN$_x$ windows. Note the SiN$_x$ windows are placed so that the sides with the window membrane come nearly into contact with each other, thereby limiting the thickness of the water layer.*
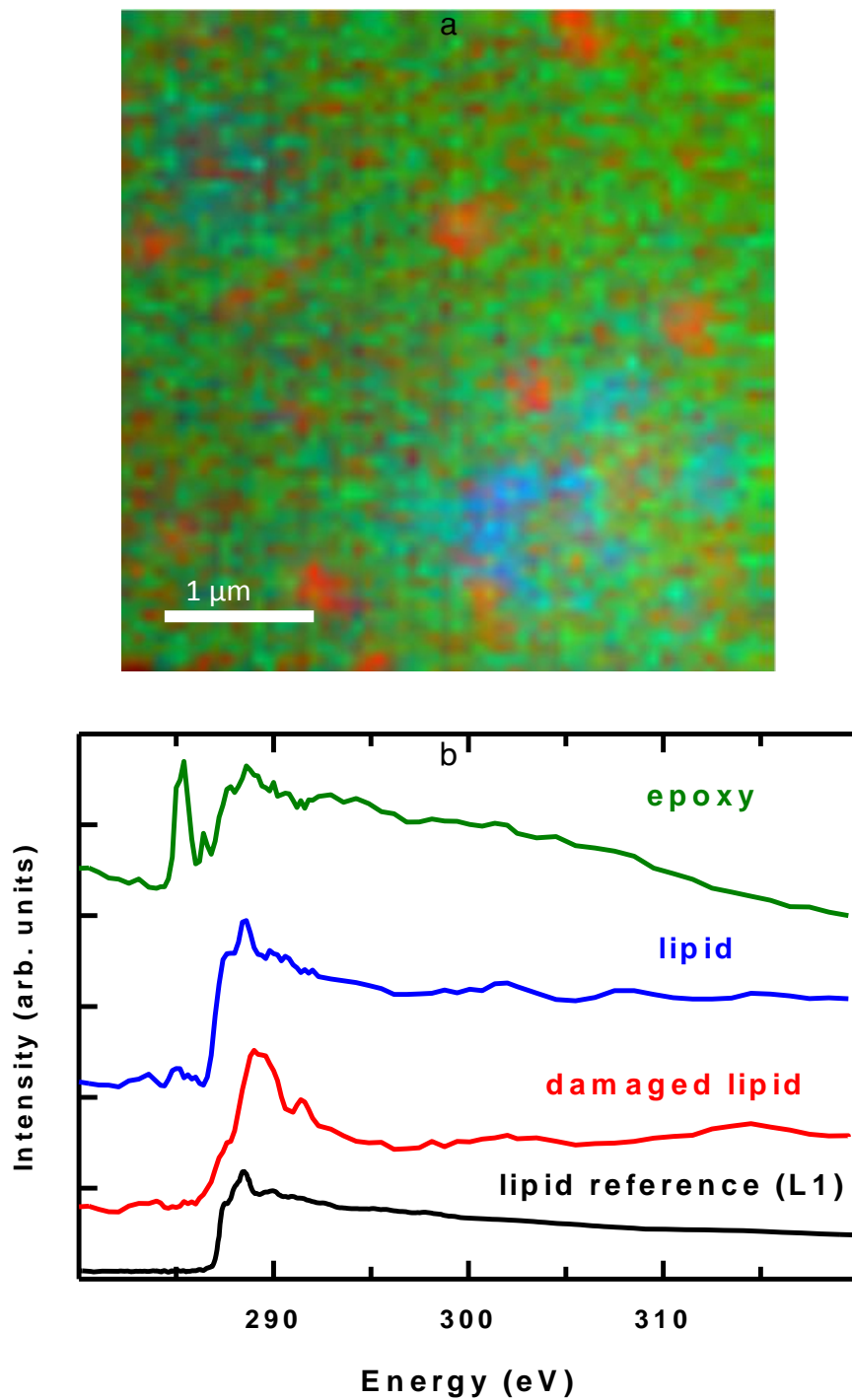
Figure 5.3. *(a) Red, green, blue (RGB) composite of the spectral maps generated by aXis 2000 for JDW006 (DOPC 50 / DSPC 50) determined from fitting a C 1s stack to the spectra in 5.3b. (b) The associated spectra generated from the different component maps.*

The results obtained from the wet cell samples suggested that sealing two silicon nitride windows together using the 5-minute curable epoxy contaminated the sample. The positive result from JDW006, was the use of Parylene-C to control the thickness of the water layer inside the two sealed windows.

5.c Improved Attempts using Hydrophilic SiN$_x$ Windows

The initial attempts at making a static wet cell showed a need to evolve from using epoxy to seal the cells and move to other techniques that eliminated the use of epoxy and would therefore mitigate that source of contamination. The focus was then shifted to the design of a flow system (Chapter 6), but other attempts were also made at creating static wet cells. These became successful after Norcada supplied proprietarily coated hydrophilic windows that better controlled the wettability of the surface. The hydrophilic coated windows from Norcada had the same dimensions but with a hydrophilic coating, removing the need for any Piranha or plasma cleaning prior to use. The Norcada hydrophilic coated windows resulted in the expected DSPC domain sizes and shapes to form (Figure 5.4) and proved to be a much more reliable substrate generating lipid bilayers than the uncoated windows.

a   DOPC 90 / DSPC 10

b   DOPC 50 / DSPC 50
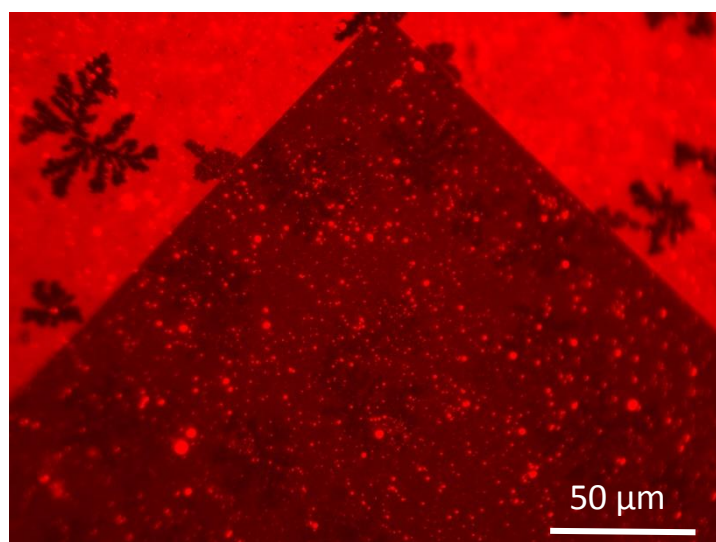
Figure 5.4. *The generation of SLBs from lipid SUVs containing various DOPC/ DSPC concentrations on the Norcada hydrophilic treated SiN$_x$ window, imaged under hydrated conditions in 1X PBS buffer.*

A static wet cell, JDW108 (DOPC 50 / DSPC 50) was constructed using the hydrophilic coated windows with a 90 second fast cure epoxy (HOME-BOND, Product Number 2040-106). The sample was imaged using FM to find suitable areas of interest for STXM. This sample was sealed in three levels of isolation with each layer in a fully saturated condition for transport to the ALS for analysis. The first attempt to analyze JDW108 using STXM showed the water level inside the wet cell was too thick for X-rays to transmit. The sample was removed from the STXM and monitored under an optical microscope while drying in an open-air environment. Later the sample was placed inside the STXM to check if the water level was thin enough for X-ray transmission. However, the sample had dried to the extent that water was no longer present, so the lipid bilayer collapsed and agglomerated, which was then analyzed. Analysis of the lipid agglomeration showed the presence of the lipid (not in the bilayer form), and the absence of any C 1s signal from epoxy. This sample showed the advantage of the 90 second curable epoxy and the hydrophilic coated windows compared to the un-coated windows.

The static wet cell samples have limitations with respect to maintaining hydration while transporting to the synchrotron radiation facilities. This is one of the advantages of a flow system, where the hydration level can be controlled both during measurement to a greater degree of precision. The need for a flow system is outlined in the following chapter. Once successfully achieved it can be applied to SLB studies under *in situ* conditions, and ultimately be extended to lipid bilayer/antimicrobial peptide interaction studies.

5.d STXM as a tool to map phase-segregated lipid bilayers

Antimicrobial peptide (AMP)/ lipid monolayer interactions have previously been studied using

STXM at a lateral spatial resolution below 80 nm [Leung, 2011]. Figure 5.5 shows the chemical

specificity and spatial resolution of STXM as applied to lipid bilayers in a static wet cell

(JDW109). It is the result of analysis of a C 1s stack measured from a region that consists of a

DSPC domain that is approximately 10 µm in diameter, in an area surrounded by DOPC, which

fluoresces red due to the addition of DHPE:LR to the sample. The fluorescent probe (DHPE-LR)

is known to preferentially partition into the liquid disordered phase, so only DOPC will appear

bright in fluorescence microscopy images [Moran-Mirabal, 2007]. The C 1s reference spectra

(Figure 3.5) for the respective lipids were used to fit the C 1s stack and thus chemically map the

distribution of the two lipid species. aXis 2000 was used to perform a "stack fit" using both of

the lipid spectra. The component maps for the individual species from this measurement are

shown in Figure 5.5. An ROI histogram selector was used to select the relevant areas in each of

the component maps from which the spectrum for the individual lipid components present

within the bilayer was generated. The conformation of the extracted DOPC and DSPC spectra to

the external DOPC and DSPC reference spectra is proof that the spatial mapping was done

correctly. It is paramount that the spectroscopy is correct so the constituent components of the

bilayer can be distinguished and ultimately differentiated from the peptides which will be

added to the system in future studies.
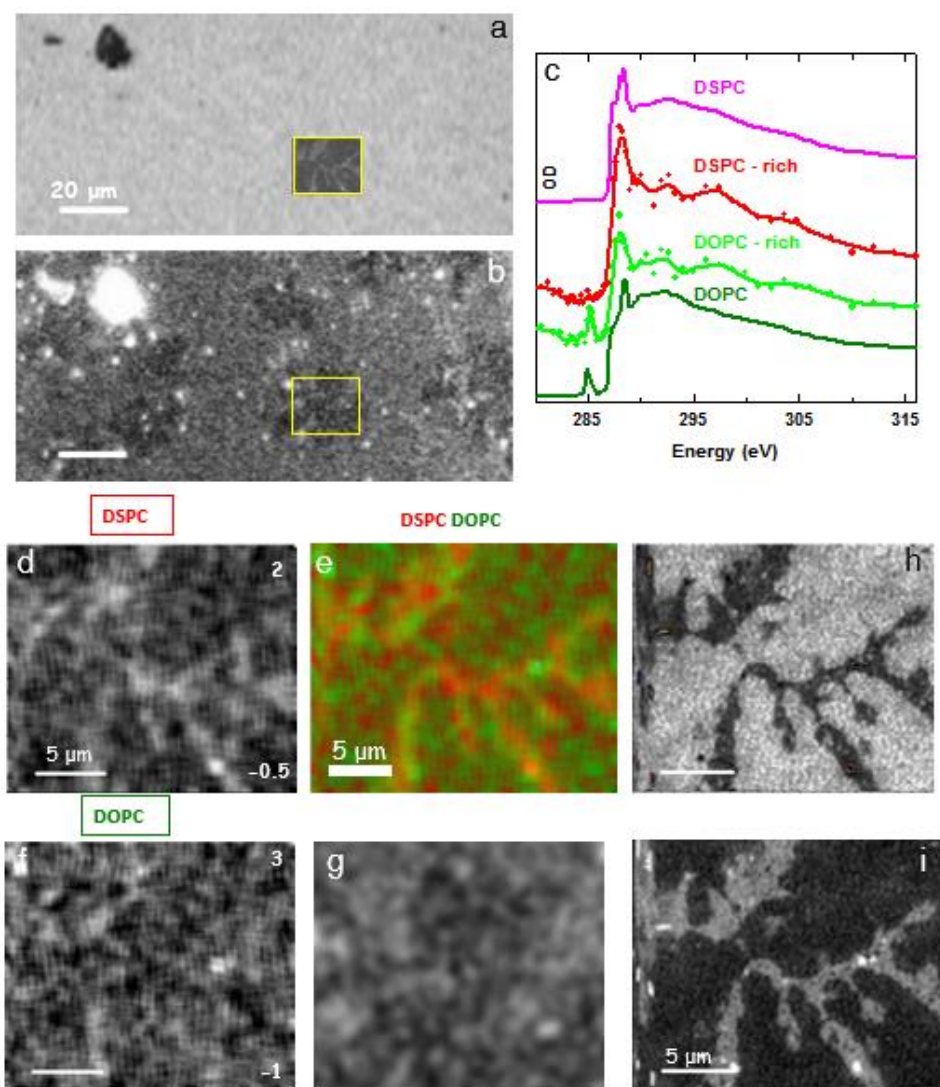
Figure 5.5. *STXM enables the chemical mapping of a binary phase-segregating lipid mixture. (a) STXM image and (b) fluorescence image (greyscale) of the same DSPC domain. The fluorescence imaging of sample JDW 109, a (50 DOPC: 50 DSPC: 0.1 DHPE- LR) bilayer was done prior to the STXM studies, to provide a clear map of a phase segregated bilayer area that contained a DSPC domain. Panel (c) Comparison of C 1s spectra extracted from the indicated regions of the DOPC 50: DSPC 50 sample with those of pure DOPC and DSPC. The raw data for the DOPC (green) and DSPC (red) rich regions are presented as scatter plots and their respective smoothed curves plotted to allow comparison against the DOPC (green) and DSPC (pink) reference spectra (cf. Figure 3.5).Panels (d) and (f) show the 2 component stack map generated by aXis 2000 after smoothing with a 5-pixel 2D Savitsky-Golay smoothing, the lipid areas are clearly seen using the DOPC and DSPC C 1s reference spectra in Figure 3.5. Panel (e) shows an RGB color composite of the DOPC and DSPC mapped areas. Panel (g) FM image of the area the C 1s stack was performed on. Panels (h) and (i) STXM images in transmission and OD respectively of the C 1s stack area, clearly indicating the DSPC domain.*

Figure 5.5 plots the DOPC and DSPC spectra that were retrieved from specific regions of the

50:50 bilayer sample (JDW 109) identified by the fit to the C 1s stack (Figure 3.5 inset) in

comparison to those of the DOPC and DSPC reference spectra. The main spectral features of

each lipid component match. The lipids can readily be distinguished by the presence/absence of

the 285.1 eV peak for the C=C 1s→π* transition which occurs in DOPC, but not in DSPC. The

maximum optical density of the JDW109 lipid bilayer sample that was measured was 0.1 OD at

the peak energy of 288.5 eV. The absorption signals from the lipid bilayer and are remarkably

small, yet all the transitions can be observed even at such a small OD. This showcases the

power of STXM as an analytical microscopy technique.

6. Towards a Flow Cell for STXM

6.a Content of this Chapter

The development of a flow cell was explored to overcome the limitations of the static wet cells

described in Chapter 5. The purpose of the flow cell is to permit lipid bilayers to maintain their

hydrated state during transport and while in the STXM and ultimately to allow addition of a

solution containing peptides, to monitor the interaction with the lipid bilayer, with or without

an applied electric field.

6.b Spatial Requirements for a Flow System Compatible with STXM

The flow cell consists of three main components: a 3D printed device attached to a STXM sample

mounting plate through which the fluid flows; a pair of interconnects to attach the inlet and

outlet tubing (purchased from IDEX Health and Science Corporation, Oak Harbor, Washington);

and a pair of Parylene-C bonded silicon nitride windows (Norcada) where the SLB is formed and

kept hydrated with a properly buffered solution and imaged with STXM.

The flow cell was constructed to be compatible with STXM, which has very restricted spatial

constraints. From the schematic in Figure 6.1, the maximum thickness of a flow device at the

level of the detector using the C 1s edge is about 4 mm at the CLS ambient STXM. This is a function

of the edge studied, as lower photon energies require smaller distances between the sample

front and the OSA (this distance is termed A_0). The A_0 for the carbon edge is ~250 μm with a 25

nm zone plate, which is typically used at CLS a-STXM and ALS STXM 5.3.2.2. The special, 3-window

SiN_x chips supplied by Norcada for this project are 500 μm thick. Since two of these chips were

bonded together (as will be explained later) on the sides containing the window membrane, a

gap of 500 µm existed between the OSA and the window, meaning that the C 1s edge could not

be imaged, but the O 1s edge could. The purpose of using these windows was to test if the overall

design would be successful and the flow of liquid could be controlled within a 3D printed device.
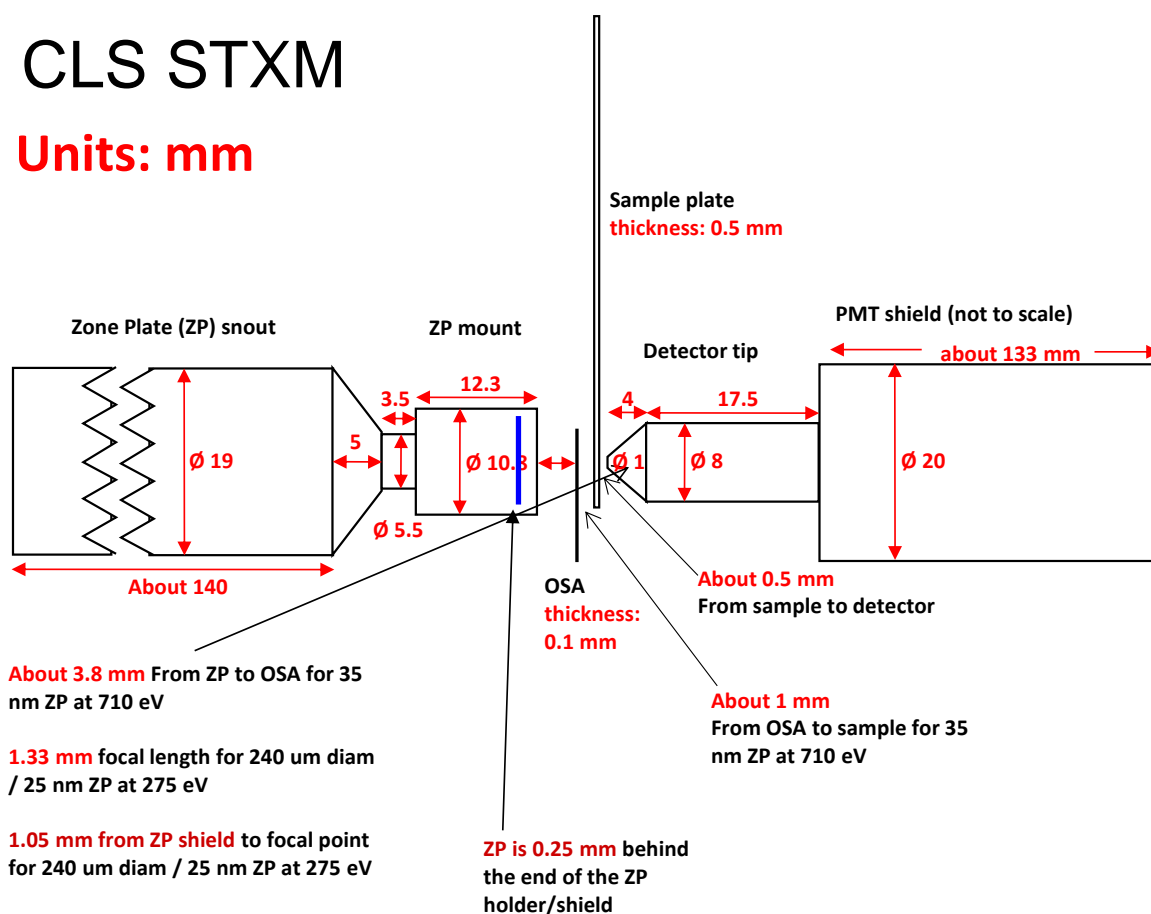
Figure 6.1. *A schematic of the STXM at the CLS. All dimensions are shown in units of mm. Adapted from Jian Wang.*

6.c Attempts to Create a Flow System Using 3D Printing

6.c.1 Extrusion Deposition 3D Printing

This part of the lipid bilayer project evolved to limit or negate the amount of epoxy required in the construction of the static wet cells that were shown to leach into the window area and contaminate the C 1s signal of the lipids that were present. 3D printing was selected as the method to fabricate a microfluidic device because of the relatively low cost associated with printing each iteration of the design. The Moran-Mirabal group purchased an extrusion deposition 3D printer (Replicator 2x, Makerbot, Brooklyn, New York, USA). An extrusion deposition printer operates by printing small beads of the material, which harden to form layers. The printer is capable of dual extrusion, meaning that it can print two types of polymers, not simultaneously, but for the same print job. This printer is capable of working with three different types of plastics: acrylonitrile butadiene styrene (ABS, Tg = 105˚C), high-impact polystyrene (HIPS, Tg = 100˚C), and polyactic acid (PLA, Tg =115˚C).

For this project, both ABS and HIPS were used. HIPS is dissolvable in limonene and therefore can be used as a support when printing hollow structures such as microfluidic channels, or components that require ABS to overhang without structural support. HIPS can be dissolved away after the device has been manufactured. The use of limonene was thought to be problematic for our manufacturing process. Limonene is an aromatic molecule which has a very strong C 1s $\rightarrow \pi*$ signal at 285 eV that would mimic the characteristic signal differentiating DOPC and DSPC. Since limonene would most likely cause contamination of the channels where lipid/peptide solutions would flow, its use was eliminated altogether, by printing only small amounts of HIPS inside the channels, which were necessary to support the ABS printing the tops of the channels. The

channels are 2 mm thick and HIPS support was printed at a thickness of 0.3 mm on each side of the channel, effectively making the channel width 1.4 mm. HIPS was also used as a support at the attachment sites of the interconnects and on the build plate of the 3D printer, on top of which the flow cell was printed in ABS. This HIPS allowed for easy removal of the flow cell from the build plate without bending the ABS printed flow cell itself.

The interconnects (IDEX Health and Science, Model N-124S) with an outer diameter of 360 µm which house the compatible olyetheretherketone (PEEK) tubing attach at the inlet and outlet. An epoxy ring from the supplier was heated with a heat gun and secured on the 3D printed device at the attachment sites of the interconnects. The interconnects make use of a rubber gasket, which provides a seal that inhibits leaking and the contamination of epoxy in the channels.
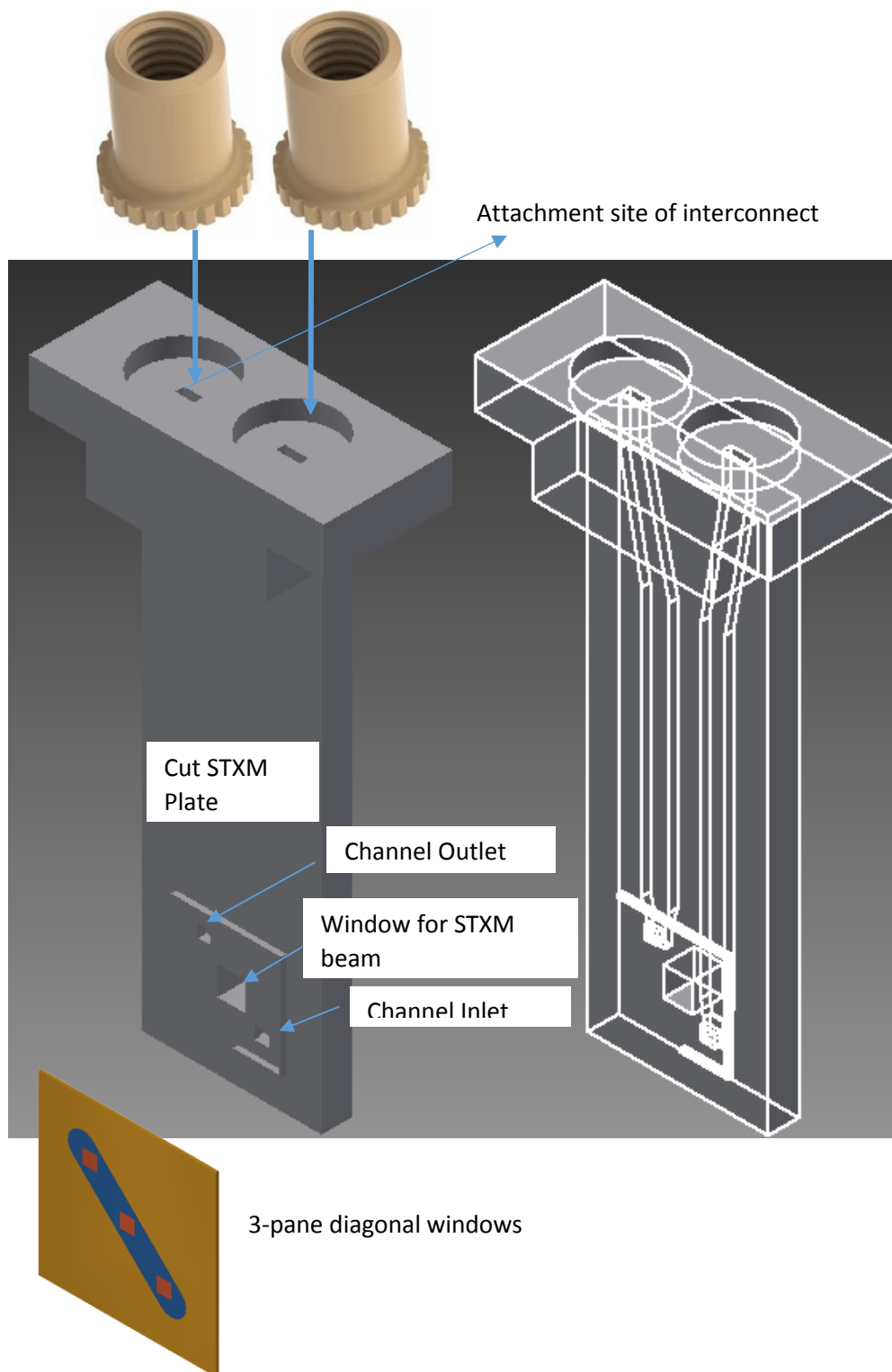
Figure 6.2 *3D computer assisted design (CAD) drawings of the 3D printed of the JDW Mark XVIII flow cell. The schematic (right) indicates the positions of the channels. The interconnects, SiN$_x$ chip and STXM plate attach to the 3D printed flow cell as indicated.*

6.c.2 Parylene-C Bonded Silicon Nitride Chips

The parylene-C precursor is commercially available as a solid material called dichloro[2.2]paracyclophane or 'dimer'. The dimer is heated under vacuum conditions allowing it to vaporize into a dimeric gas. The gas is then thermochemically degraded (pyrolized), cleaving the dimer into its radical monomeric form. The deposition takes place inside a chemical vapour deposition chamber (Specialty Coating System, Indianapolis, Indiana), where the monomer polymerizes into a conformal and pinhole-free thin film on surfaces at lower temperatures. The thickness of the film is controlled by the amount of parylene-C dimer that is added to the vapourization chamber [Noh, 2004].

Parylene-C was deposited onto two SiN_x windows featuring 3 window areas along the diagonal and a spacer layer (Norcada, Edmonton, Alberta) – Figure 6.3. A physical mask was placed on both of the windows during deposition to define the chanel shape. The Parylene-coated windows were bonded by heating to 190˚C for 2 hours while putting pressure on the frame on the window frames [Ziegler, 2006].
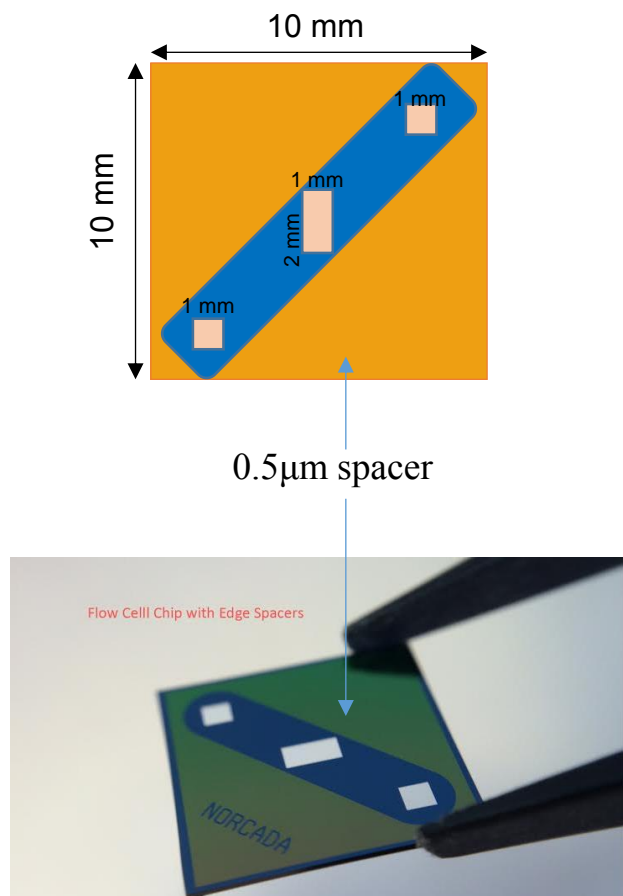
Figure 6.3 *Illustration with dimensions (left) and picture (right) of the silicon nitride windows used for the 3D printed flow cell device.*

The thickness of the frame is 0.50 mm and the thickness of each window is 100 nm. The Parylene was coated on top of the 0.5 μm spacer and then bonded together. The thickness of the Parylene deposited on each silicon nitride chip was approximately 500 nm, giving a total channel thickness of about 2 μm. The thickness needed to be limited because soft x-rays in the C 1s region can only penetrate through a maximum of 1-2 μm of water. The Parylene bonded chips were then secured to the 3D printed cell using O-ring gaskets to ensure a fluid-tight seal. Epoxy was placed around the frame of the SiN_x chip and the SiN_x chip guide on the 3D printed device to ensure a seal between the two components. Since the OSA is only 250 μm away from the sample, nothing could be placed on the front of the chip, leaving epoxy as the only option to ensure a seal.

Figure 6.4 shows the predicted transmission of X-rays through water and SiN_x on various thicknesses. A 5 μm thick water layer only has ~20% transmission in the carbon, region as opposed to a 1 μm thickness layer of water which has ~65% transmission in the same region. Ideal optical densities for spectroscopy are near 1 OD, while anything above an OD of 2 will have absorption saturation. 100 nm thick SiN_x windows with a 500 nm to 1000 nm water thickness provide the ideal conditions for spectroscopy at the C 1s edge.
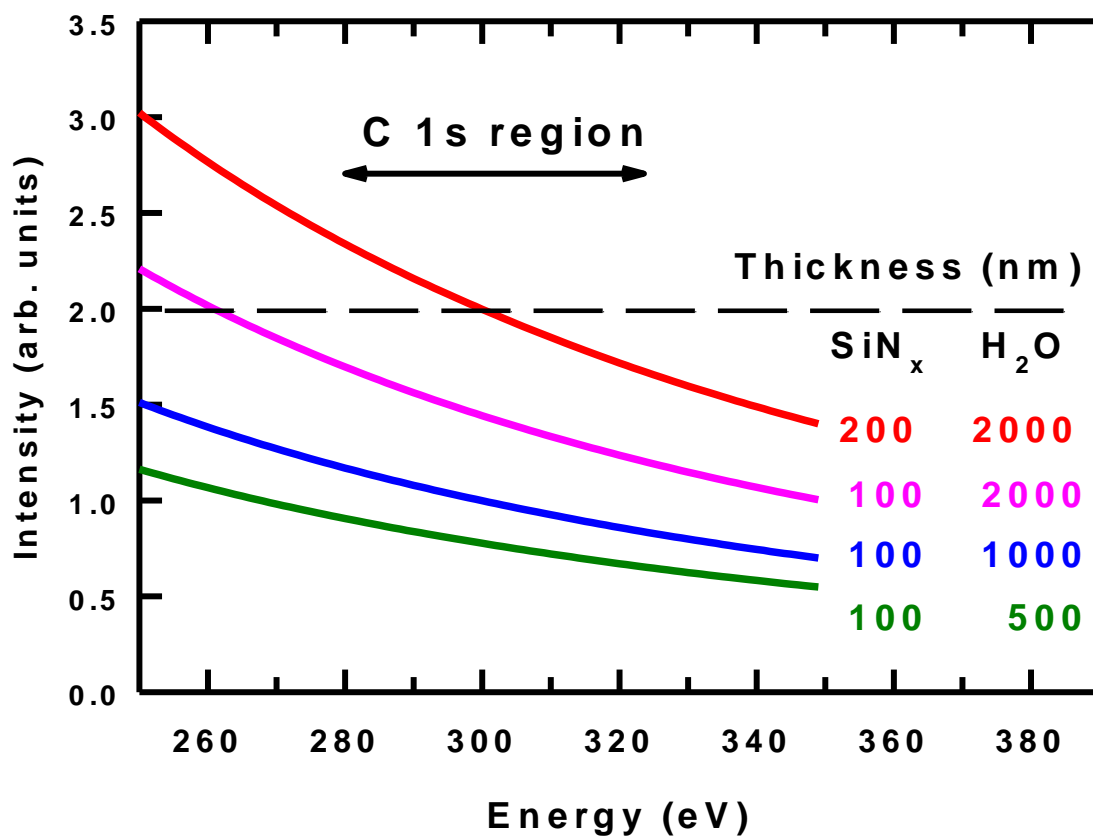
Figure 6.4. *The predicted transmission of X-rays in the carbon region (270-350 eV) through various thicknesses of water and SiN$_x$ windows.*

The first test of the completed flow cell occurred at the ALS STXM 5.3.2.2 on 11 May, 2015. There were several problems that needed to be addressed. There was a leak between the seal of the SiN_x chips and the 3D printed device, which occurred because (i) the rubber gaskets had a thickness of 0.25 μm, which prevented contact between the SiN_x chip and the 3D printed flow cell and (ii), the surface of the 3D printed device was not entirely smooth, even after it was sanded with fine grain sand paper, followed by smoothing with a Kim Wipe containing isopropyl alcohol.

The thickness of the JDW Mark XVIII device at the SiN_x chip guide area was 3.2 mm, not including the 1 mm pair of bonded SiN_x windows. Initially, the STXM plate was attached to the rear of the 3D printed flow cell, however, the interferometer would not engage because the coarse-Z (distance between the front surface of the sample plate holder and the OSA) was 5000 μm. The minimum distance for the coarse-Z to engage the interferometer is 3500 μm. A standard STXM plate was cut horizontally 4 mm above the tops of slots 1-3 and secured to the flow cell. This setup with the partial STXM plate mounted on the front of the flow cell allowed the interferometer to engage.

The flow cell was filled with deionized water and an O 1s energy stack was performed. Water was observed along with contaminants on the surface of the window. When the cell was removed from the STXM tank, a leak through the back of the 3D printed device was noted and water was observed on the rear of the viewing window. Therefore, it was unknown if the water filled the channel between the SiN_x windows during the O 1s stack, or was present on the rear of the window.

6.d Conclusions from the 3D Printed Flow Cell

Constructing a flow cell with an extrusion deposition printer with a maximum resolution of 100 µm and a poor surface smoothness were the main reasons this technique proved ineffective. The tolerances of the printer proved to be insufficient relative to the degree of precision required for a successful design. Additionally, the use of epoxy did not create a water-tight seal between the components, which caused leaks. Had the surface of the 3D printed device been smoother, O-ring grooves could have been constructed at the interface between the SiN_x chip and the 3D printed device. Thin O-rings would have provided a better seal, so long as ultrathin wire (less than 200 µm) was used to clamp the SiN_x chip to the device. This design would have required SiN_x chips with a larger geometry (12 mm x 12 mm, as opposed to 10 mm x 10 mm) to ensure the wire would not come into contact with the OSA. These 12 mm x 12 mm SiN_x chips were designed on CAD software to have a thickness of 200 µm, so the C 1s edge could be analyzed. The design was forwarded to Norcada, but weighing the cost of the proposed chips to the limitations associated with extrusion deposition 3D printing, it was decided that an alternative approach seemed like a more worthwhile option.

7. Summary & Suggestions for Future Studies

7.a Summary of thesis

This project was built upon work of Yujie Zhu, a PhD student in the Moran-Mirabal lab, who had made lipid samples for STXM. These samples had varying degrees of success, and Yujie often characterized the SLB samples she prepared using fluorescence and atomic force microscopy. This project furthered the work that Yujie initiated in particular, by (i) devising a refined procedure for the reliable formation of SLBs (ii) getting reliable lipid reference spectra, and (iii) exploring fabrication of a flow cell. The SLB preparation was optimized to ensure effective sample preparation and control of the domain size of DSPC. This optimized procedure will be useful in future studies.

The generation of valid X-ray absorption reference spectroscopy for the C 1s, N 1s and O1s edges of three lipids used to prepare SLBs has enabled us to map lipid bilayers in their dried state. This was accomplished using the features associated with saturated and unsaturated lipid species of the C 1s reference spectra. This thesis has also shown that STXM can map very low OD (~0.02OD peak) bilayer spectra and extract spectra from multicomponent lipid bilayers that conform to the established reference spectra. The combination of fluorescence microscopy and STXM was used to map the same area using both techniques, which can provide information from the micrometer scale to the 100 nanometer scale.

A graduate student in the Hitchcock lab, Vinod Prabu is currently developing an electrochemical flow cell that is compatible with STXM. The flow cell is being constructed using ultra-high definition 3D printing, which has a resolution of 25 µm and is intended to be compatible with a

Norcada (Edmonton, Alberta) designed, hydrophilic coated SiN_x window capable of controlling the thickness of the electrolyte fluid layer to between 75-100 nm. Systems with flow that are STXM compatible have already been achieved, although (at the time of writing this thesis) the fluid thickness layer is still too large (>10 μm) for studies at the C 1s edge. As of June, 2016 Vinod has made advances with the electrochemical flow cell and has been able to exchange water for a $CuSO_4$ aqueous solution. This result is very promising as it shows the ability to control the flow of fluids in minimal volumes. The electrolyte solution is critical for electrochemical flow cell applications and translates to being able to control the distribution of fluid when the electrochemical flow cell is adapted for use with SLBs.

Once the (electrochemical) flow cell has proven to be functional, it is the intention to apply it to lipid bilayer experiments, where the SLBs will be formed on the SiN_x window, kept hydrated in a properly buffered environment and examined at the C 1s edge at the ALS and CLS. Ultimately, it should be possible to extend the experiment to include adding antimicrobial peptides into the SLB system.

7.b Future Studies

7.b.1 Recommendations

In this author's opinion, improvements to the SLB formation procedure (and the lipid reference spectroscopy procedure) should still be made. A single Hamilton glass syringe should be dedicated to each lipid, rather than rinsing five times with chloroform when changing lipid species. This should enhance the reliability of SLB formation. Negatively charged lipids should be explored because these will be used as a mimic of prokaryotic lipid bilayers.

To achieve a more accurate analysis of the size of the DSPC domains, AFM can be used to probe

SLBs. This can be done both with hydrated and dried SLBs and one could measure the drying

effect on the size of the SLBs.

7.b.2 Future Work

Once a reliable flow cell is developed, it can be implemented for lipid bilayer/antimicrobial

peptide studies. Future experiments should prepare and characterize mixed saturated-

unsaturated lipid bilayers. The next step will be to flow a solution of peptides through the device

and monitor the interactions between the two. Since the charges of the CAMPs and the

negatively charged lipid bilayer are believed to be what drives the interaction, the third step will

be to apply a transverse electric field to see if that affects the propensity, or sites of CAMP

binding. The ability to apply electric fields in STXM has been shown previously [Guay, 2005].

Multiple lipids may be used in future experiments to alter the charge of the layer to which the

peptides will bind. Antimicrobial peptides are known to be cationic and will therefore bind more

readily to an anionic bilayer. Manipulating the charge of the lipid bilayer itself by controlling the

pH of the environment using a buffer or using charged lipids will allow control over the

interactions between the cAMP and the bilayer.

Antimicrobial peptide/lipid monolayer interactions have been studied previously using STXM at

a lateral spatial resolution below 80 nm (Leung, 2011). However, these studies were not

performed under hydrated *in situ* conditions. The flow cell is the optimal device to characterize

the AMP/lipid bilayer interactions under hydrated *in situ* conditions using STXM. Peptides have

a dominant C 1s $\rightarrow \pi^*_{C=O}$ transition at 288.2 eV [Leung, 2011] that is sufficiently different from the C 1s $\rightarrow \pi^*_{C=O-O}$ peak of lipids (288.5 eV) to be differentiable [Lawrence, 2003].

There are considerable challenges associated with this experiment. These include (i) the ability of the flow cell to control the fluid layer thickness to be thin enough for photons to transmit, but also for the bilayer to remain hydrated; (ii) radiation damage directly to the lipids, and as a corollary of the radiolysis of water which can generate free radicals that have the ability to react with the species has been noted in the literature [Tzvetkov, 2009]; (iii) the very weak absorption signal of single lipid bilayers at the C 1s edge is 0.02 OD at the 288.5 eV peak. The low absorption signal means that for both I and I_0 very good statistics and minimum systematic noise are required. Although there are clear challenges associated with this experiment, if it can be successful, it may improve our understanding of the antimicrobial/antibacterial properties of peptides, which is of paramount concern, as we continue to see bacteria become more resistant to currently available antibiotics [WHO, 2016]. This thesis provides the necessary background information and foundation for these challenging, yet scientifically valuable experiments.

References

Adams, Peter G., Kirstie L. Swingle, Walter F. Paxton, John J. Nogan, Loreen R. Stromberg, Millicent A. Firestone, Harshini Mukundan, and Gabriel A. Montaño. "Exploiting Lipopolysaccharide-Induced Deformation of Lipid Bilayers to Modify Membrane Composition and Generate Two-Dimensional Geometric Membrane Array Patterns." *Scientific Reports* 5 (May 27, 2015): 10331. doi:10.1038/srep10331.

Alekshun, Michael N., and Stuart B. Levy. "Molecular Mechanisms of Antibacterial Multidrug Resistance." *Cell* 128, no. 6 (March 23, 2007): 1037–50. doi:10.1016/j.cell.2007.03.004.

Alexander Fleming Discovery and Development of Penicillin - Landmark - American Chemical Society." Accessed May 1, 2015. http://www.acs.org/content/acs/en/education/whatischemistry/landmarks/flemingpenicillin.html.

Andersson, Jakob, and Ingo Köper. "Tethered and Polymer Supported Bilayer Lipid Membranes: Structure and Function." *Membranes* 6, no. 2 (2016): 30.

Andersen, Olaf S., and II Roger E. Koeppe. "Bilayer Thickness and Membrane Protein Function: An Energetic Perspective." *Annual Review of Biophysics and Biomolecular Structure* 36, no. 1 (2007): 107–30. doi:10.1146/annurev.biophys.36.040306.132643.

Attwood, David. *Soft x-rays and extreme ultraviolet radiation: principles and applications*. Cambridge university press, 2007.

Auras, Rafael A., Loong-Tak Lim, Susan E. M. Selke, and Hideto Tsuji. *Poly(lactic Acid): Synthesis, Structures, Properties, Processing, and Applications*. John Wiley & Sons, 2011.
"Impact Resistance - Tips for Plastic Material Selection." Accessed May 1, 2015. http://www.plasticprop.com/articles/impact-resistance-tips-plastic-material-selection.

Avanti Polar Lipids. Materials Safety Data Sheet: DOPC 850375C 07/30/2015. https://avantilipids.com/images/MSDS/AvantiPolarLipids_SDS_850375C.pdf . Accessed April 2, 2016.

Benzerara, K., T. H. Yoon, T. Tyliszczak, B. Constantz, A. M. Spormann, and G. E. Brown. "Scanning Transmission X-Ray Microscopy Study of Microbial Calcification." *Geobiology* 2, no. 4 (October 1, 2004): 249–59. doi:10.1111/j.1472-4677.2004.00039.x.

Brogden, Kim A. "Antimicrobial Peptides: Pore Formers or Metabolic Inhibitors in Bacteria?" *Nature Reviews Microbiology* 3, no. 3 (March 2005): 238–50. doi:10.1038/nrmicro1098.

Brown, C. M., K. L. Klein, D. V. Krogstad, G. A. Myers, and A. A. Herzing. "Transmission Electron Microscopy of Lipid Vesicles in Liquid Cells." *Microscopy and Microanalysis* 20, no. S3 (2014): 1334–1335.

Chao, Weilun, Peter Fischer, T. Tyliszczak, Senajith Rekawa, Erik Anderson, and Patrick Naulleau. "Real space soft x-ray imaging at 10 nm spatial resolution." *Optics express* 20, no. 9 (2012): 9777-9783.

Cody, G. D., Harald Ade, S. Wirick, G. D. Mitchell, and A. Davis. "Determination of Chemical-Structural Changes in Vitrinite Accompanying Luminescence Alteration Using C-NEXAFS Analysis." *Organic Geochemistry* 28, no. 7 (1998): 441–455.

Hernández Cruz, Daniel, Marie-Eve Rousseau, Marcia M. West, Michel Pézolet, and Adam P. Hitchcock. "Quantitative Mapping of the Orientation of Fibroin β-Sheets in B. M Ori Cocoon Fibers by Scanning Transmission X-Ray Microscopy." *Biomacromolecules* 7, no. 3 (2006): 836–843.

Dhople, Vishnu, Amy Krukemeyer, and Ayyalusamy Ramamoorthy. "The Human Beta-Defensin-3, an Antibacterial Peptide with Multiple Biological Functions." *Biochimica et Biophysica Acta (BBA) - Biomembranes*, Membrane Biophysics of Antimicrobial Peptides, 1758, no. 9 (September 2006): 1499–1512. doi:10.1016/j.bbamem.2006.07.007.

Gordon, Michelle L., Glyn Cooper, Cynthia Morin, Tohru Araki, Cassia C. Turci, Konstantin Kaznatcheev, and Adam P. Hitchcock. "Inner-Shell Excitation Spectroscopy of the Peptide Bond: Comparison of the C 1s, N 1s, and O 1s Spectra of Glycine, Glycyl-Glycine, and Glycyl-Glycyl-Glycine." *The Journal of Physical Chemistry A* 107, no. 32 (2003): 6144–6159.

Guay, Daniel, Jacob Stewart-Ornstein, Xuerong Zhang, and Adam P. Hitchcock. "In Situ Spatial and Time-Resolved Studies of Electrochemical Reactions by Scanning Transmission X-Ray Microscopy." *Analytical Chemistry* 77, no. 11 (June 1, 2005): 3479–87. doi:10.1021/ac048077j.

Habets, Michelle G. J. L., and Michael A. Brockhurst. "Therapeutic Antimicrobial Peptides May Compromise Natural Immunity." *Biology Letters*, January 25, 2012, rsbl20111203. doi:10.1098/rsbl.2011.1203.

Hancock, Robert E. W., and Hans-Georg Sahl. "Antimicrobial and Host-Defense Peptides as New Anti-Infective Therapeutic Strategies." *Nature Biotechnology* 24, no. 12 (December 2006): 1551–57. doi:10.1038/nbt1267.

Henke, Burton L., Eric M. Gullikson, and John C. Davis. "X-ray interactions: photoabsorption, scattering, transmission, and reflection at E= 50-30,000 eV, Z= 1-92." *Atomic data and nuclear data tables* 54, no. 2 (1993): 181-342.

Henzler Wildman, Katherine A., Dong-Kuk Lee, and A. Ramamoorthy. "Mechanism of Lipid Bilayer Disruption by the Human Antimicrobial Peptide, LL-37†." *Biochemistry* 42, no. 21 (June 1, 2003): 6545–58. doi:10.1021/bi0273563.

Hitchcock, A. P., and D. C. Mancini. "Bibliography and Database of Inner Shell Excitation Spectra of Gas Phase Atoms and Molecules." *Journal of Electron Spectroscopy and Related Phenomena* 67, no. 1 (March 18, 1994): vii. doi:10.1016/0368-2048(93)02024-G.

Hitchcock, Adam P. Soft X-Ray Imaging and Spectromicroscopy." In *Handbook of Nanoscopy*, edited by Gustaaf Van Tendeloo, Dirk Van Dyck, and Stephen J. Pennycook, 745–91. Wiley-VCH Verlag GmbH & Co. KGaA. 2012. http://onlinelibrary.wiley.com/doi/10.1002/9783527641864.ch22/summary.

Hoskin, David W., and Ayyalusamy Ramamoorthy. "Studies on Anticancer Activities of Antimicrobial Peptides." *Biochimica et Biophysica Acta (BBA) - Biomembranes* 1778, no. 2 (February 2008): 357–75. doi:10.1016/j.bbamem.2007.11.008.

Howells, Malcolm, Christopher Jacobsen, Tony Warwick, and A. Van den Bos. "Principles and Applications of Zone Plate X-Ray Microscopes." In *Science of Microscopy*, edited by Peter W. Hawkes and John C. H. Spence, 835–926. Springer New York, 2007. http://link.springer.com/chapter/10.1007/978-0-387-49762-4_13.

Jacobsen, C., John M. Kenney, J. Kirz, R. J. Rosser, F. Cinotti, H. Rarback, and J. Pine. "Quantitative Imaging and Microanalysis with a Scanning Soft X-Ray Microscope." *Physics in Medicine and Biology* 32, no. 4 (1987): 431.

Jacobsen, Chris. "Soft X-Ray Microscopy." *Trends in Cell Biology* 9, no. 2 (1999): 44–47.

Kaznatcheev, K. V., Ch Karunakaran, U. D. Lanke, S. G. Urquhart, M. Obst, and A. P. Hitchcock. "Soft X-ray spectromicroscopy beamline at the CLS: commissioning results." *Nuclear Instruments and Methods in Physics Research Section A: Accelerators, Spectrometers, Detectors and Associated Equipment* 582, no. 1 (2007): 96-99.

Koenig, Bernd W., and Klaus Gawrisch. "Specific Volumes of Unsaturated Phosphatidylcholines in the Liquid Crystalline Lamellar Phase." *Biochimica et Biophysica Acta (BBA)-Biomembranes* 1715, no. 1 (2005): 65–70.

Konyakhina, Tatyana M., Jing Wu, James D. Mastroianni, Frederick A. Heberle, and Gerald W. Feigenson. "Phase Diagram of a 4-Component Lipid Mixture: DSPC/DOPC/POPC/chol." *Biochimica et Biophysica Acta* 1828, no. 9 (September 2013): 2204–14. doi:10.1016/j.bbamem.2013.05.020.

Korlach, Jonas, Petra Schwille, Watt W. Webb, and Gerald W. Feigenson. "Characterization of Lipid Bilayer Phases by Confocal Microscopy and Fluorescence Correlation Spectroscopy." *Proceedings of the National Academy of Sciences* 96, no. 15 (1999): 8461–8466.

A.L.D. Kilcoyne, T. Tylisczak, W.F. Steele, S. Fakra, P. Hitchcock, K. Franck, E. Anderson, B. Harteneck, E.G. Rightor, G.E. Mitchell, A. P. Hitchcock, L. Yang, T. Warwick, H. Ade, *Interferometrically controlled Scanning Transmission Microscopes at the Advanced Light Source*, J. Synchrotron Radiation 10 (2003) 125-136

Kučerka, Norbert, Stephanie Tristram-Nagle, and John F. Nagle. "Structure of Fully Hydrated Fluid Phase Lipid Bilayers with Monounsaturated Chains." *The Journal of Membrane Biology* 208, no. 3 (2006): 193–202.

Kučerka, Norbert, Mu-Ping Nieh, and John Katsaras. "Fluid phase lipid areas and bilayer thicknesses of commonly used phosphatidylcholines as a function of temperature." *Biochimica et Biophysica Acta (BBA)-Biomembranes* 1808, no. 11 (2011): 2761-2771.

Larson, Elaine. "Community Factors in the Development of Antibiotic Resistance." *Annual Review of Public Health* 28, no. 1 (2007): 435–47 doi:10.1146/annurev.publhealth.28.021406.144020.

Lawrence, J. R., G. D. W. Swerhone, G. G. Leppard, T. Araki, X. Zhang, M. M. West, and A. P. Hitchcock. "Scanning Transmission X-Ray, Laser Scanning, and Transmission Electron Microscopy Mapping of the Exopolymeric Matrix of Microbial Biofilms." *Applied and Environmental Microbiology* 69, no. 9 (2003): 5543–5554.

Lehmann, Johannes, Biqing Liang, Dawit Solomon, Mirna Lerotic, Flavio Luizão, James Kinyangi, Thorsten Schäfer, Sue Wirick, and Chris Jacobsen. "Near-edge X-ray absorption fine structure (NEXAFS) spectroscopy for mapping nano-scale distribution of organic carbon forms in soil: Application to black carbon particles." *Global Biogeochemical Cycles* 19, no. 1 (2005).

Leung, Bonnie O., Adam P. Hitchcock, Amy Won, Anatoli Ianoul, and Andreas Scholl. "Imaging Interactions of Cationic Antimicrobial Peptides with Model Lipid Monolayers Using X-Ray Spectromicroscopy." *European Biophysics Journal* 40, no. 6 (2011): 805–810.

Leung, Bonnie O., John L. Brash, and Adam P. Hitchcock. "Characterization of Biomaterials by Soft X-Ray Spectromicroscopy." *Materials* 3, no. 7 (2010): 3911–3938.

Lewis, Barbara A., and Donald M. Engelman. "Lipid Bilayer Thickness Varies Linearly with Acyl Chain Length in Fluid Phosphatidylcholine Vesicles." *Journal of Molecular Biology* 166, no. 2 (1983): 211–217.

Mabrey, S, and J M Sturtevant. "Investigation of Phase Transitions of Lipids and Lipid Mixtures by Sensitivity Differential Scanning Calorimetry." *Proceedings of the National Academy of Sciences of the United States of America* 73, no. 11 (November 1976): 3862–66.

Mashaghi, S.; Jadidi, T.; Koenderink, G.; Mashaghi, A. Lipid Nanotechnology. *International Journal of Molecular* Sciences. 2013,14, 4242–4282. doi:10.3390/ijms14024242.

Matsuzaki, Katsumi, Kenichi Sugishita, Nobutaka Fujii, and Koichiro Miyajima. "Molecular Basis for Membrane Selectivity of an Antimicrobial Peptide, Magainin 2." *Biochemistry* 34, no. 10 (March 1, 1995): 3423–29. doi:10.1021/bi00010a034.

Matsuzaki, Katsumi. "Control of Cell Selectivity of Antimicrobial Peptides." *Biochimica et Biophysica Acta (BBA) - Biomembranes*, Amphibian Antimicrobial Peptides, 1788, no. 8 (August 2009): 1687–92. doi:10.1016/j.bbamem.2008.09.013.

Moran-Mirabal, Jose M., Donald M. Aubrecht, and Harold G. Craighead. "Phase Separation and Fractal Domain Formation in Phospholipid/diacetylene-Supported Lipid Bilayers." *Langmuir* 23, no. 21 (2007): 10661–10671.

Morin, Cynthia. "Soft X-ray Spectromicroscopy of Proteins on Patterned Polymer Films." PhD Thesis. McMaster University. October 2004.

Nagle, John F., and Stephanie Tristram-Nagle. "Structure of Lipid Bilayers." *Biochimica et Biophysica Acta (BBA)-Reviews on Biomembranes* 1469, no. 3 (2000): 159–195.

Najafi, Ebrahim, Daniel Hernández Cruz, Martin Obst, Adam P. Hitchcock, Bastien Douhard, Jean-Jacques Pireaux, and Alexandre Felten. "Polarization Dependence of the C 1s X-Ray Absorption Spectra of Individual Multi-Walled Carbon Nanotubes." *Small* 4, no. 12 (2008): 2279–2285.

Neu, T.R., B. Manz, F. Volke, J.J. Dynes, A.P. Hitchcock and J.R. Lawrence. *Advanced imaging techniques for assessment of structure, composition and function in biofilm systems*. FEMS Microbiology Ecology   72 (2010) 1–21.

Nguyen, Leonard T., Evan F. Haney, and Hans J. Vogel. "The Expanding Scope of Antimicrobial Peptide Structures and Their Modes of Action." *Trends in Biotechnology* 29, no. 9 (September 2011): 464–72. doi:10.1016/j.tibtech.2011.05.001.

Noh, Hong-Seok, Yong Huang, and Peter J. Hesketh. "Parylene Micromolding, a Rapid and Low-Cost Fabrication Method for Parylene Microchannel." *Sensors and Actuators B: Chemical* 102, no. 1 (September 2004): 78–85. doi:10.1016/j.snb.2003.09.038.

Oh, Min Ho, Eun Kil Park, Sung Min Kim, Jaeyeong Heo, and Hyeong Joon Kim. "Long-Term Stability of SiNx Thin-Film Barriers Deposited by Low Temperature PECVD for OLED." *ECS Journal of Solid State Science and Technology* 5, no. 5 (2016): R55-R58.

O'Driscoll, Noelle H., Olga Labovitiadi, T. P. Tim Cushnie, Kerr H. Matthews, Derry K. Mercer, and Andrew J. Lamb. "Production and Evaluation of an Antimicrobial Peptide-Containing Wafer Formulation for Topical Application." *Current Microbiology* 66, no. 3 (November 25, 2012): 271–78. doi:10.1007/s00284-012-0268-3.

Papo, N., and Y. Shai. "Host Defense Peptides as New Weapons in Cancer Treatment." *Cellular and Molecular Life Sciences CMLS* 62, no. 7–8 (April 1, 2005): 784–90. doi:10.1007/s00018-005-4560-2.

Peschel, Andreas, Michael Otto, Ralph W. Jack, Hubert Kalbacher, Günther Jung, and Friedrich Götz. "Inactivation of the Dlt Operon inStaphylococcus Aureus Confers Sensitivity to Defensins, Protegrins, and Other Antimicrobial Peptides." *Journal of Biological Chemistry* 274, no. 13 (March 26, 1999): 8405–10. doi:10.1074/jbc.274.13.8405.

Peters, Brian M., Mark E. Shirtliff, and Mary Ann Jabra-Rizk. "Antimicrobial peptides: primeval molecules or future drugs?." *PLoS Pathog* 6, no. 10 (2010): e1001067.

Rankin, David WH. "CRC Handbook of Chemistry and Physics, Edited by David R. Lide," 2009. http://www.tandfonline.com/doi/full/10.1080/08893110902764125.

Reddy, K. V. R.; Yedery, R. D.Aranha, C. Antimicrobial Peptides: Premises and Promises. *International Journal of Antimicrobial Agents* 2004, 24, no. 6 536–547. doi:10.1016/j.ijantimicag.2004.09.005.

Ridler, TW & Calvard, S (1978), "Picture thresholding using an iterative selection method", IEEE Transactions on Systems, Man and Cybernetics 8: 630-632

Rightor, E. G., A. P. Hitchcock, H. Ade, R. D. Leapman, S. G. Urquhart, A. P. Smith, G. Mitchell, D. Fischer, H. J. Shin, and T. Warwick. "Spectromicroscopy of Poly(ethylene Terephthalate): Comparison of Spectra and Radiation Damage Rates in X-Ray Absorption and Electron Energy Loss." *The Journal of Physical Chemistry B* 101, no. 11 (March 1, 1997): 1950–60. doi:10.1021/jp9622748.

Rühl, E., A. T. Wen, and A. P. Hitchcock. "Inner-Shell Excitation of η5-C5H5Co(CO)2 and Related Compounds Studied by Gas Phase Electron Energy Loss Spectroscopy." *Journal of Electron Spectroscopy and Related Phenomena* 57, no. 2 (October 1, 1991): 137–64. doi:10.1016/0368-2048(91)85020-T.

Sabnis, Ram Wasudeo. *Handbook of Biological Dyes and Stains: Synthesis and Industrial Applications*. John Wiley & Sons, 2010.

Simons, Kai, and Winchil LC Vaz. "Model Systems, Lipid Rafts, and Cell Membranes 1." *Annu. Rev. Biophys. Biomol. Struct.* 33 (2004): 269–295.

Sloan, Courtney D. Kuhnline, Michael T. Marty, Stephen G. Sligar, and Ryan C. Bailey. "Interfacing Lipid Bilayer Nanodiscs and Silicon Photonic Sensor Arrays for Multiplexed Protein–lipid and Protein–membrane Protein Interaction Screening." *Analytical Chemistry* 85, no. 5 (2013): 2970–2976.

Szoka Jr, Frank, and Demetrios Papahadjopoulos. "Comparative Properties and Methods of Preparation of Lipid Vesicles (Liposomes)." *Annual Review of Biophysics and Bioengineering* 9, no. 1 (1980): 467–508.

Tzvetkov, George, Paulo Fernandes, Stephan Wenzel, Andreas Fery, Gaio Paradossi, and Rainer H. Fink. "Soft X-Ray Induced Modifications of PVA-Based Microbubbles in Aqueous Environment: A Microspectroscopy Study." *Physical Chemistry Chemical Physics* 11, no. 7 (2009): 1098–1104.

Tzong-Hsien Lee, Christine Heng, Marcus J. Swann, John D. Gehman, Frances Separovic, Marie-Isabel Aguilar, Real time quantitative analysis of lipid disordering by aurein 1.2 during membrane adsorption, destabilisation and lysis, . Biochimica et Biophysica Acta (BBA) - Biomembranes, Volume 1798, Issue 10, October 2010, Pages 1977-1986.

Urquhart, S. G., and H. Ade. "Trends in the carbonyl core (C 1s, O 1s)→ π* C= O transition in the near-edge X-ray absorption fine structure spectra of organic molecules." *The Journal of Physical Chemistry B* 106, no. 34 (2002): 8531-8538.

van Swaay, Dirk. "Microfluidic methods for forming liposomes." *Lab on a Chip* 13, no. 5 (2013): 752-767.

Walheim, Stefan, Martin Böltau, Jürgen Mlynek, Georg Krausch, and Ullrich Steiner. "Structure Formation via Polymer Demixing in Spin-Cast Films." *Macromolecules* 30, no. 17 (August 1, 1997): 4995–5003. doi:10.1021/ma9619288.

Wan, Jiamin, Tolek Tyliszczak, and Tetsu K. Tokunaga. "Organic Carbon Distribution, Speciation, and Elemental Correlations within Soil Microaggregates: Applications of STXM and NEXAFS Spectroscopy." *Geochimica et Cosmochimica Acta* 71, no. 22 (2007): 5439–5449.
J. Wang, G.A. Botton, M.M. West and A.P. Hitchcock, *Quantitative evaluation of radiation damage to polyethylene terephthalate by soft X-rays and high energy electrons,* J. Phys. Chem B 113 (2009) 1869–1876.

Warwick, T., K. Franck, J. B. Kortright, G. Meigs, M. Moronne, S. Myneni, E. Rotenberg, et al. "A Scanning Transmission X-Ray Microscope for Materials Science Spectromicroscopy at the Advanced Light Source." *Review of Scientific Instruments* 69, no. 8 (1998): 2964–2973.

Warwick, Tony, Harald Ade, David Kilcoyne, Michael Kritscher, Tolek Tyliszczak, Sirine Fakra, Adam Hitchcock, Peter Hitchcock, and Howard Padmore. "A new bend-magnet beamline for scanning transmission X-ray microscopy at the Advanced Light Source." *Journal of synchrotron radiation* 9, no. 4 (2002): 254-257.

"WHO | WHO's First Global Report on Antibiotic Resistance Reveals Serious, Worldwide Threat to Public Health." *WHO*. Accessed March 11, 2016. http://www.who.int/mediacentre/news/releases/2014/amr-report/en/.

Won, Amy, Mourin Khan, Sorin Gustin, Akuvi Akpawu, Deeptee Seebun, Tyler J. Avis, Bonnie O. Leung, Adam P. Hitchcock, and Anatoli Ianoul. "Investigating the effects of L-to D-amino acid substitution and deamidation on the activity and membrane interactions of antimicrobial peptide anoplin." *Biochimica et Biophysica Acta (BBA)-Biomembranes* 1808, no. 6 (2011): 1592-1600.

Yeaman, Michael R., and Nannette Y. Yount. "Mechanisms of Antimicrobial Peptide Action and Resistance." *Pharmacological Reviews* 55, no. 1 (March 1, 2003): 27–55. doi:10.1124/pr.55.1.2.

Zasloff, Michael. "Antimicrobial Peptides of Multicellular Organisms." *Nature* 415, no. 6870 (January 24, 2002): 389–95. doi:10.1038/415389a.

Ziegler, Dominik, T. Suzuki, and S. Takeuchi. "Fabrication of Flexible Neural Probes With Built-In Microfluidic Channels by Thermal Bonding of Parylene." *Journal of Microelectromechanical Systems* 15, no. 6 (December 2006): 1477–82. doi:10.1109/JMEMS.2006.879681.

Zhu, Yujie. "Piranha Cleaning." May 2014. http://www.chemistry.mcmaster.ca/moran-mirabal/resources/PIRANHA-CLEAN-5-2014.pdf

Zhu, Yujie. "Supported Bilayer Preparation." August 2015. http://www.chemistry.mcmaster.ca/moran-mirabal/resources/SUPPORTED-LIPID-BILAYER-PREPARATION-SOP-9-2015.pdf